STABILITY OF COMPRESSIBLE BOUNDARY LAYERS

Ali H. Nayfeh
Department of Engineering Science and Mechanics
Virginia Polytechnic Institute and State University
Blacksburg, VA

ABSTRACT

The stability of compressible two- and three-dimensional boundary layers is reviewed. The stability of 2D compressible flows differs from that of incompressible flows in two important features: There is more than one mode of instability contributing to the growth of disturbances in supersonic laminar boundary layers and the most unstable first-mode wave is three-dimensional. Whereas viscosity has a destabilizing effect on incompressible flows, it is stabilizing for high supersonic Mach numbers. Whereas cooling stabilizes first-mode waves, it destabilizes second-mode waves. However, second-order waves can be stabilized by suction and favorable pressure gradients. The influence of the nonparallelism on the spatial growth rate of disturbances is evaluated. The growth rate depends on the flow variable as well as the distance from the body. Floquet theory is used to investigate the subharmonic secondary instability.

1. INTRODUCTION

The aim of this paper is to review the state of the art of the stability of compressible boundary layers. The study discusses the influence of Mach number, Reynolds number, cooling, suction, pressure gradients, wave angle, and nonparallelism. Subharmonic secondary instability is also discussed.

The earliest attempt at formulating a compressible stability theory was made by Kuchemann (ref. 1) who neglected viscosity, the mean temperature gradient, and the curvature of the mean velocity profile. Lees and Lin (ref. 2) and Lees (ref. 3) were the first to derive the basic equations for the linear parallel stability analysis of compressible boundary layers. This theory was extended by Dunn and Lin (ref. 4), Reshotko (ref. 5), and Lees and Reshotko (ref. 6). These early theories were asymptotic or approximate in nature and proved to be valid only up to low supersonic Mach numbers. The use of direct computer solutions to exploit the full compressible stability equations was initiated by Brown (ref. 7) and Mack (ref. 8). An extensive treatment of the parallel stability theory for compressible flows is given by Mack (refs. 9-15). As the Mach number increases, the dissipation terms become important and a three-dimensional disturbance cannot be treated by an equivalent two-dimensional method as is usually done for the incompressible case. Mack (refs. 10,15) found that neglecting the dissipation terms can lead to a 10% error in the disturbance amplification rate.

It is an interesting facet of compressible two-dimensional boundary layers that the most unstable first-mode wave need not be parallel to the freestream as the Mach number approaches one. At supersonic speeds the most unstable first-mode wave is oblique or three-dimensional.

The most important feature of the stability of supersonic laminar boundary layers is that there can be more than one mode of instability contributing to the growth of the disturbance. The first mode is similar to the Tollmien-Schlichting instability mode of incompressible flows, while the second and higher unstable modes are unique to compressible flows. Mack (ref. 10) found that there are multiple

values of wave numbers for a single disturbance phase velocity whenever there is a region of supersonic mean flow relative to the disturbance phase velocity. For incompressible flows, higher modes are associated with higher wave numbers at different phase speeds. In contrast with the first mode, the most unstable second mode is two-dimensional. As the Mach number increases to the hypersonic regime, the second mode displays growth rates that are higher than those of the three-dimensional first mode. However, the maximum growth rate is less than that of the first mode at zero Mach number.

These stability theories treat the mean flows as quasiparallel flows. Some incomplete attempts to account for the nonparallel flow effects by including either the normal velocity or some of the streamwise derivatives of the mean flow were given by Brown (ref. 16), Gunness (ref. 17), and Boehman (ref. 18). Complete nonparallel theories for two-dimensional flows were developed by El-Hady and Nayfeh (ref. 19) and Gaponov (20) and for three-dimensional flows by Nayfeh (21) and El-Hady (22). The growth rate in a parallel flow is independent of the flow variable and the distance from the wall, whereas the growth rate in a nonparallel flow (growing boundary layer) depends on the flow variable and the distance from the wall. This complicates the interpretation of experimental data for comparison with the results of stability theory.

In contrast with the case of incompressible flows, rigorous stability experiments are very difficult at supersonic speeds because (a) the spatial and temporal resolution of instruments at supersonic speeds is less than those at low speeds, (b) with the exception of Kendall, experimenters have less control and knowledge of the disturbances at supersonic speeds, and (c) the interference of traversing probes at high speeds is due to the high aerodynamic loads which necessitate strong and bulky walls. Therefore, most of the information on the stability of high-speed flows is macroscopic rather than microscopic. The term macroscopic refers to measurements of the onset of turbulence and the extent of the transition region, whereas the term microscopic refers to measurements of the evolution in space and time of the fluctuations present in the flow that are sufficient for the identification of the instabilities that lead to transition and the validation of the proposed theoretical models. It should be noted that macroscopic experiments are difficult to relate directly to stability theory, whereas microscopic experiments, which provide information about the unstable disturbances and their growth, can be better related to stability theory, which studies the development of individual components of the disturbances corresponding to a certain frequency or a wavepacket. Thus, microscopic experiments that use controlled disturbances are more desirable for corroboration with theory than experiments that study natural disturbances arising from one source or another in the boundary layer. The natural disturbances represent a set of space and time components, whereas controlled experiments can provide disturbances with a given frequency and a given spanwise wavenumber.

Whereas experimenters developed various credible techniques to introduce controlled artificial disturbances in incompressible boundary layers, the technique of Kendall seems to be the only credible technique at supersonic speeds. Laufer and Vrebalovich (ref. 23) used a high-speed valve and Demetriades used a siren mechanism attached to a flat plate to introduce their artificial disturbances. The valve opened and closed a narrow slit in the surface of the plate to allow periodic air pulses of certain frequency to disturb the boundary layer. Kendall introduced small artificial disturbances by a glow discharge between two electrodes embedded in the surface of the flat plate skewed at a specified angle to the spanwise direction,

thereby introducing disturbances with a specified wave angle. The rest of the available experiments were performed using natural disturbances.

Almost all measurements reported on the experimental stability of boundary layers were made by means of either hot-wire anemometers or hot films following disturbances in these boundary layers. The hot-wire response is a combination of velocity, density, and temperature fluctuations. The hot-wire response when operated at high constant overheat is proportional to the mean square of the mass-flow fluctuations. To describe the disturbance fully, one needs measurements of all fluctuation characteristics such as the rms amplitude, spectra, and propagation speed as functions of both y and x. Almost all reported experiments for compressible flows measured $|\rho u|$ at various x-stations by placing hot wires or hot films at a transverse location where the mean-flow conditions are the same. Laufer and Vrebalovich (ref. 23) reported measurements at different constant y/L positions, while Kendall (refs. 24,25), Demetriades (refs. 26-28), Lebiga et al (ref. 29), and Stetson, Thompson, Donaldson and Siler (refs. 30-33) reported measurements at one constant y/L located in the wideband energy peak.

Laufer and Vrebalovich (ref. 23) carried out measurements of the neutral stability curves, amplification rates, wavelengths, and amplitude distributions at the Mach numbers 1.6 and 2.2. They performed their measurements in the JPL 20" supersonic wind tunnel where the freestream turbulence level was reduced to about 1% by means of damping screens. Laufer and Vrebalovich performed their measurements for natural as well as artificial disturbances. The stability characteristics of natural disturbances in supersonic flows at Mach numbers between 1.6 and 8.5 were examined by Kendall (refs. 24,25) in the JPL 20" supersonic wind tunnel. In some of these experiments, the side walls of the tunnel were turbulent and hence radiated sound. Mack (ref. 12) tried to compare the free oscillations in the parallel stability theory with Kendall's data. The comparison was satisfactory only for the case $M_\infty = 4.5$. In an attempt to account for the response of the boundary layer to the incoming sound waves, Mack (ref. 12) included a forcing term at the first neutral stability point and found a better agreement with Kendall's data. The same characteristic features of the boundary-layer response to the incoming sound waves were observed by Lebiga et al (ref. 29) in their experiments at $M_\infty = 2$. Demetriades (refs. 26,27) presented experimental results for hypersonic boundary-layer flows. He studied the streamwise amplitude variation of both natural disturbances and disturbances artificially excited with a siren mechanism attached to a flat plate.

2. PROBLEM FORMULATION

In this paper, we consider the linear quasi-parallel as well as the nonparallel stability of two- and three-dimensional compressible boundary layers. Moreover, we consider the linear secondary instability of two-dimensional primary waves in a two-dimensional compressible boundary layer. The basic equations for the linear stability analysis of parallel-flow compressible boundary layers were first derived by Lees and Lin (ref. 2), Lees (ref. 3), and Dunn and Lin (ref. 4), using the small disturbance theory. For excellent references on the compressible parallel stability theory, we refer the reader to the papers of Mack. For the nonparallel theory of compressible boundary layers, we refer the reader to the papers by El-Hady and Nayfeh (ref. 19) and Nayfeh (ref. 21).

Lengths, velocities, and time are made dimensionless using a suitable reference length L^*, the freestream velocity U^*_∞, and L^*/U^*_∞, respectively. The pressure is made dimensionless using $\rho^*_\infty U^{*2}_\infty$, where ρ^*_∞ is the freestream density. The temperature, density, specific heats, viscosity, and thermal conductivity are made dimensionless

using their corresponding freestream values. The gas is assumed to be perfect. Since the pressure is constant across the boundary layer

$$\rho_m T_m = 1 \text{ and } p_m = \frac{1}{\gamma M_\infty^2} \qquad (2.1)$$

where the subscript m refers to mean flow quantities, γ is the ratio of the specific heats of the gas, and M_∞ is the freestream Mach number.

To formulate the problem so that the disturbance equations can be specialized to all these cases, we assume the basic flow to be a time-dependent three-dimensional flow and superpose on it small disturbances to obtain total flow quantities of the form

$$\hat{q}(x,y,z,t) = q_b(x,y,z,t) + q(x,y,z,t) \qquad (2.2)$$

Here $q_b(x,y,z,t)$ stands for a basic state quantity and $q(x,y,z,t)$ stands for a small unsteady disturbance. Substituting the total flow quantities $\hat{u}$, $\hat{v}$, $\hat{w}$, $\hat{\rho}$, $\hat{p}$, $\hat{\mu}$, and $\hat{T}$ into the Navier-Stokes equations, subtracting the basic state, and linearizing, we find to first order that the disturbance equations are given by

$$\frac{\partial \rho}{\partial t} + \frac{\partial}{\partial x}(\rho_b u + \rho u_b) + \frac{\partial}{\partial y}(\rho_b v + \rho v_b) + \frac{\partial}{\partial z}(\rho_b w + \rho w_b) = 0 \qquad (2.3)$$

$$\rho_b \left(\frac{\partial u}{\partial t} + u_b \frac{\partial u}{\partial x} + u \frac{\partial u_b}{\partial x} + v_b \frac{\partial u}{\partial y} + v \frac{\partial u_b}{\partial y} + w_b \frac{\partial u}{\partial z} + w \frac{\partial u_b}{\partial z} \right) + \rho \left(\frac{\partial u_b}{\partial t} \right.$$

$$+ u_b \frac{\partial u_b}{\partial x} + v_b \frac{\partial u_b}{\partial y} + w_b \frac{\partial u_b}{\partial z} \right) = -\frac{\partial p}{\partial x} + \frac{1}{R} \left\{ \frac{\partial}{\partial x} \left[\mu_b \left(r \frac{\partial u}{\partial x} + m \frac{\partial v}{\partial y} + m \frac{\partial w}{\partial z} \right) \right. \right.$$

$$\left. + \mu \left(r \frac{\partial u_b}{\partial x} + m \frac{\partial v_b}{\partial y} + m \frac{\partial w_b}{\partial z} \right) \right] + \frac{\partial}{\partial y} \left[\mu_b \left(\frac{\partial u}{\partial y} + \frac{\partial v}{\partial x} \right) + \mu \left(\frac{\partial u_b}{\partial y} + \frac{\partial v_b}{\partial x} \right) \right]$$

$$+ \frac{\partial}{\partial z} \left[\mu_b \left(\frac{\partial w}{\partial x} + \frac{\partial u}{\partial z} \right) + \mu \left(\frac{\partial w_b}{\partial x} + \frac{\partial u_b}{\partial z} \right) \right] \right\} \qquad (2.4)$$

$$\rho_b \left(\frac{\partial v}{\partial t} + u_b \frac{\partial v}{\partial x} + u \frac{\partial v_b}{\partial x} + v_b \frac{\partial v}{\partial y} + v \frac{\partial v_b}{\partial y} + w_b \frac{\partial v}{\partial z} + w \frac{\partial v_b}{\partial z} \right) + \rho \left(\frac{\partial v_b}{\partial t} + u_b \frac{\partial v_b}{\partial x} \right.$$

$$+ v_b \frac{\partial v_b}{\partial y} + w_b \frac{\partial v_b}{\partial z} \right) = -\frac{\partial p}{\partial y} + \frac{1}{R} \left\{ \frac{\partial}{\partial x} \left[\mu_b \left(\frac{\partial u}{\partial y} + \frac{\partial v}{\partial x} \right) + \mu \left(\frac{\partial u_b}{\partial y} + \frac{\partial v_b}{\partial x} \right) \right] \right.$$

$$+ \frac{\partial}{\partial y} \left[\mu_b \left(m \frac{\partial u}{\partial x} + r \frac{\partial v}{\partial y} + m \frac{\partial w}{\partial z} \right) + \mu \left(m \frac{\partial u_b}{\partial x} + r \frac{\partial v_b}{\partial y} + m \frac{\partial w_b}{\partial z} \right) \right]$$

$$+ \frac{\partial}{\partial z} \left[\mu_b \left(\frac{\partial v}{\partial z} + \frac{\partial w}{\partial y} \right) + \mu \left(\frac{\partial v_b}{\partial z} + \frac{\partial w_b}{\partial y} \right) \right] \right\} \qquad (2.5)$$

632

$$\rho_b\left(\frac{\partial w}{\partial t} + u_b\frac{\partial w}{\partial x} + u\frac{\partial w_b}{\partial x} + v_b\frac{\partial w}{\partial y} + v\frac{\partial w_b}{\partial y} + w_b\frac{\partial w}{\partial z} + w\frac{\partial w_b}{\partial z}\right) + \rho\left(\frac{\partial w_b}{\partial t} + u_b\frac{\partial w_b}{\partial x}\right.$$

$$\left. + v_b\frac{\partial w_b}{\partial y} + w_b\frac{\partial w_b}{\partial z}\right) = -\frac{\partial p}{\partial z} + \frac{1}{R}\left\{\frac{\partial}{\partial x}\left[\mu_b\left(\frac{\partial w}{\partial x} + \frac{\partial u}{\partial z}\right) + \mu\left(\frac{\partial w_b}{\partial x} + \frac{\partial u_b}{\partial z}\right)\right]\right.$$

$$+ \frac{\partial}{\partial y}\left[\mu_b\left(\frac{\partial v}{\partial z} + \frac{\partial w}{\partial y}\right) + \mu\left(\frac{\partial v_b}{\partial z} + \frac{\partial w_b}{\partial y}\right)\right] + \frac{\partial}{\partial z}\left[\mu_b\left(m\frac{\partial u}{\partial x} + m\frac{\partial v}{\partial y}\right.\right.$$

$$\left.\left.\left. + r\frac{\partial w}{\partial z}\right)\right] + \frac{\partial}{\partial z}\left[\mu\left(m\frac{\partial u_b}{\partial x} + m\frac{\partial v_b}{\partial y} + r\frac{\partial w_b}{\partial z}\right)\right]\right\} \tag{2.6}$$

$$\rho_b\left[\frac{\partial T}{\partial t} + u\frac{\partial T_b}{\partial x} + u_b\frac{\partial T}{\partial x} + v\frac{\partial T_b}{\partial y} + v_b\frac{\partial T}{\partial y} + w\frac{\partial T_b}{\partial z} + w_b\frac{\partial T}{\partial z}\right]$$

$$+ \rho\left[\frac{\partial T_b}{\partial t} + u_b\frac{\partial T_b}{\partial x} + v_b\frac{\partial T_b}{\partial y} + w_b\frac{\partial T_b}{\partial z}\right] = (\gamma - 1)M_\infty^2\left[\frac{\partial p}{\partial t} + u\frac{\partial p_b}{\partial x} + u_b\frac{\partial p}{\partial x}\right.$$

$$\left. + v_b\frac{\partial p}{\partial y} + w\frac{\partial p_b}{\partial z} + w_b\frac{\partial p}{\partial z} + \frac{1}{R}\Phi\right] + \frac{1}{R Pr}\left\{\frac{\partial}{\partial x}\left(\mu_b\frac{\partial T}{\partial x} + \mu\frac{\partial T_b}{\partial x}\right)\right.$$

$$\left. + \frac{\partial}{\partial y}\left(\mu_b\frac{\partial T}{\partial y} + \mu\frac{\partial T_b}{\partial y}\right) + \frac{\partial}{\partial z}\left(\mu_b\frac{\partial T}{\partial z} + \mu\frac{\partial T_b}{\partial z}\right)\right\} \tag{2.7}$$

$$\frac{p}{p_b} = \frac{T}{T_b} + \frac{\rho}{\rho_b} \tag{2.8}$$

where Φ is the perturbation dissipation function defined by

$$\Phi = \mu_b\left\{2r\left(\frac{\partial u_b}{\partial x}\frac{\partial u}{\partial x} + \frac{\partial v_b}{\partial y}\frac{\partial v}{\partial y} + \frac{\partial w_b}{\partial z}\frac{\partial w}{\partial z}\right) + 2m\left[\frac{\partial u_b}{\partial x}\left(\frac{\partial v}{\partial y} + \frac{\partial w}{\partial z}\right)\right.\right.$$

$$\left. + \frac{\partial v_b}{\partial y}\left(\frac{\partial u}{\partial x} + \frac{\partial w}{\partial z}\right) + \frac{\partial w_b}{\partial z}\left(\frac{\partial u}{\partial x} + \frac{\partial v}{\partial y}\right)\right] + 2\left(\frac{\partial u}{\partial y} + \frac{\partial v}{\partial x}\right)\left(\frac{\partial u_b}{\partial y} + \frac{\partial v_b}{\partial x}\right)$$

$$+ 2\left(\frac{\partial u}{\partial z} + \frac{\partial w}{\partial x}\right)\left(\frac{\partial u_b}{\partial z} + \frac{\partial w_b}{\partial x}\right) + 2\left(\frac{\partial v}{\partial z} + \frac{\partial w}{\partial y}\right)\left(\frac{\partial v_b}{\partial z} + \frac{\partial w_b}{\partial y}\right)\right\} + \mu\left\{r\left[\left(\frac{\partial u_b}{\partial x}\right)^2\right.\right.$$

$$\left. + \left(\frac{\partial v_b}{\partial y}\right)^2 + \left(\frac{\partial w_b}{\partial z}\right)^2\right] + 2m\left[\frac{\partial u_b}{\partial x}\frac{\partial v_b}{\partial y} + \frac{\partial u_b}{\partial y}\frac{\partial w_b}{\partial z} + \frac{\partial v_b}{\partial y}\frac{\partial w_b}{\partial z}\right]$$

$$\left. + \left(\frac{\partial u_b}{\partial y} + \frac{\partial v_b}{\partial x}\right)^2 + \left(\frac{\partial u_b}{\partial z} + \frac{\partial w_b}{\partial x}\right)^2 + \left(\frac{\partial v_b}{\partial z} + \frac{\partial w_b}{\partial y}\right)^2\right\} \tag{2.9}$$

The constants r and m are given by

$$r = \frac{2}{3}(e + 2) \quad \text{and} \quad m = \frac{2}{3}(e - 1) \tag{2.10}$$

where e = 0 corresponds to the Stokes hypothesis. The Reynolds number R and Prandtl number Pr are given by

$$R = \frac{U_\infty^* L_\infty^*}{\nu_\infty^*}, \quad Pr = \frac{\mu_\infty^* c_p^*}{\kappa_\infty^*} \tag{2.11a}$$

where ν_∞^*, μ_∞^*, and κ_∞^* are the freestream kinematic viscosity, dynamic viscosity, and thermal conductivity, respectively, and c_p^* is the dimensional specific heat at constant pressure. We assume that the dynamic viscosity is a function of the temperature only so that

$$\mu = T \left. \frac{d\mu_b}{dT} \right|_{T_b} \tag{2.11b}$$

The boundary conditions at the wall are

$$u = v = w = T = 0 \quad \text{at} \quad y = 0 \tag{2.12}$$

The boundary conditions on the velocity fluctuations u and w represent the no-ship conditions and the boundary condition on the velocity fluctuation v represents the no-penetration condition. For a gas flowing over a solid wall, the temperature remains at its mean value unless the frequency is small (i.e., stationary or near stationary disturbances). The boundary conditions as $y \to \infty$ are

$$u(y), \ v(y), \ w(y), \ p(y), \text{ and } T(y) \text{ are bounded as } y \to \infty \tag{2.13}$$

As will be described later, neutral subsonic disturbances decay to zero as $y \to \infty$, whereas neutral supersonic disturbances do not vanish as $y \to \infty$.

3. QUASIPARALLEL PRIMARY INSTABILITY

In this section, we consider the three-dimensional stability of a steady three-dimensional boundary layer. In general, the mean flow in a boundary layer varies with the streamwise coordinate x and spanwise coordinate z. However, at high Reynolds numbers, this variation is small over distances the order of the wavelengths of the disturbances. Consequently, most stability analyses neglect the streamwise and spanwise variations of the mean flow, the so-called parallel-flow assumption. Thus, the basic flow is approximated by

$$u_b = U_m(y), \ v_b = 0, \ w_b = W_m(y), \ T_b = T_m(y), \ p_b = P_m(x) \tag{3.1}$$

Using the parallel-flow assumption reduces equations (2.3)-(2.9) to a system of linear partial differential equations whose coefficients vary only with y. Consequently, the variables t, x, and z can be separated using the so-called normal mode assumption

$$[u,v,p,T,w] = [\zeta_1(y), \ \zeta_3(y), \ \zeta_4(y), \ \zeta_5(y), \ \zeta_7(y)] \ \exp[i(\alpha x + \beta z - \omega t)] \tag{3.2}$$

where α and β are the wave numbers in the streamwise and spanwise directions, respectively, and ω is the frequency. For a temporal stability, α and β are real

but ω is complex. For spatial stability, ω is real but α and β are complex. For the general case, α, β, and ω are complex.

Substituting equations (3.1) and (3.2) into equations (2.3)-(2.9), (2.12), and (2.13) yields the eigenvalue problem

$$D\zeta_3 + i\alpha\zeta_1 - \frac{DT_m}{T_m}\zeta_3 + i(\alpha U_m + \beta W_m - \omega)\left(\gamma M_\infty^2\zeta_4 - \frac{\zeta_5}{T_m}\right)$$
$$+ i\beta\zeta_7 = 0 \tag{3.3}$$

$$i(\alpha U_m + \beta W_m - \omega)\zeta_1 + \zeta_3 DU_m + i\alpha T_m\zeta_4 - \frac{T_m}{R}\{- \mu_m(r\alpha^2 + \beta^2)\zeta_1$$
$$- \alpha\beta\mu_m(m+1)\zeta_7 + i(m+1)\alpha\mu_m D\zeta_3 + \mu_m'D\zeta_1 + i\alpha\mu_m'\zeta_3$$
$$+ \mu_m D^2\zeta_1 + D(\mu_m'DU_m)\zeta_5 + \mu_m'DU_m D\zeta_5\} = 0 \tag{3.4}$$

$$i(\alpha U_m + \beta W_m - \omega)\zeta_3 + T_m D\zeta_4 - \frac{T_m}{R}\{i(m+1)\alpha\mu_m D\zeta_1$$
$$+ im\alpha\mu_m'\zeta_1 - (\alpha^2 + \beta^2)\mu_m\zeta_3 + r\mu_m'D\zeta_3 + im\beta\mu_m'\zeta_7$$
$$+ i\alpha\mu_m'DU_m\zeta_5 + i\beta\mu_m'DW_m\zeta_5 + r\mu_m D^2\zeta_3 + i(m+1)\beta\mu_m D\zeta_7\} = 0 \tag{3.5}$$

$$i(\alpha U_m + \beta W_m - \omega)\zeta_7 + \zeta_3 DW_m + i\beta T_m\zeta_4 - \frac{T_m}{R}\{- (m+1)\alpha\beta\mu_m\zeta_1$$
$$+ i\beta\mu_m'\zeta_3 + i(m+1)\beta D\zeta_3 - \mu_m(\alpha^2 + r\beta^2)\zeta_7 + \mu_m'D\zeta_7 + \mu_m D^2\zeta_7\} = 0 \tag{3.6}$$

$$i(\alpha U_m + \beta W_m - \omega)\zeta_5 + \zeta_3 DT_m - i(\gamma - 1)T_m M_\infty^2(\alpha U_m + \beta W_m - \omega)\zeta_4$$
$$- \frac{T_m}{R}\left[2DU_m(D\zeta_1 + i\alpha\zeta_3) + 2DW_m(i\beta\zeta_3 + D\zeta_7) + \mu_m'(DU_m)^2\zeta_5\right.$$
$$\left.+ \mu_m'(DW_m)^2\zeta_5\right] - \frac{T_m}{RPr}\left[- \mu_m(\alpha^2 + \beta^2)\zeta_5 + D(\mu_m D\zeta_5) + D(\mu_m'DT_m\zeta_5)\right] = 0 \tag{3.7}$$

$$\zeta_1 = \zeta_3 = \zeta_5 = \zeta_7 = 0 \quad \text{at} \quad y = 0 \tag{3.8}$$

$$\zeta_n \text{ are bounded as } y \to \infty \tag{3.9}$$

where $D = \partial/\partial y$.

Introducing the Stuart transformation (ref. 34)

$$k\eta_1 = \alpha\zeta_1 + \beta\zeta_7 \tag{3.10}$$

$$k\eta_7 = \alpha\zeta_7 - \beta\zeta_1 \tag{3.11}$$

where $k = \sqrt{\alpha^2 + \beta^2}$ does not reduce the eighth-order system (3.3)-(3.9) into a sixth-order system due to the coupling in the energy equation due to a single dissipation terms, which couples the energy equation to the other equations for 3D waves in 2D or 3D boundary layers. Neglecting this term reduces the eigenvalue problem from an eight-order complex problem to a sixth-order complex problem, thereby resulting in a large saving in computations. The error introduced to this simplification is a function of the Mach number, Reynolds number, and wave angle. For the case of insulated flat plates, Mack found that the maximum error is less than 5% for all Mach numbers at R = 1500. However, most stability calculations being formed are based on the eighth-order rather than the sixth-order system.

Two methods of solution have been employed (refs. 11,35,36). The first reduces the system of equations (3.3)-(3.7) into an eighth-order system of ordinary differential equations, determines an exact solution outside the boundary layer that satisfies the boundary conditions (3.9), uses the resulting linearly independent solutions as initial conditions to integrate the first-order equations to the wall, employs a Gram-Schmidt orthonormalization scheme to keep the solutions linearly independent, and uses an iterative scheme such as Newton-Raphson procedure to determine the desired complex eigenvalue. The second method uses a finite-difference scheme to reduce the governing equations into a system of algebraic equations that is solved using standard techniques to determine the desired eigenvalue.

According to the first approach, the eigenvalue problem (3.3)-(3.9) is converted into a system of first-order equations by letting

$$\zeta_2 = Du = D\zeta_1, \quad \zeta_6 = DT = D\zeta_5, \quad \text{and} \quad \zeta_8 = Dw = D\zeta_7 \tag{3.12}$$

Then, the eigenvalue problem becomes

$$D\zeta = F(y)\zeta \tag{3.13a}$$

$$\zeta_1 = \zeta_3 = \zeta_5 = \zeta_7 = 0 \quad \text{at} \quad y = 0 \tag{3.13b}$$

$$\zeta_n \text{ are bounded as } y \to \infty \tag{3.13c}$$

where $\zeta^T = \{\zeta_1, \zeta_2, \ldots, \zeta_8\}$ and the elements a_{ij} of the matrix F are given in Appendix A. For a given R and a mean flow U_m, W_m, and T_m, the eigenvalue problem (3.13) provides a dispersion relation of the form

$$\omega = \omega(\alpha, \beta) \tag{3.14}$$

In general, ω, α, and β are complex. Thus, equation (3.14) provides two relations among the six real parameters α_r, α_i, β_r, β_i, ω_r, and ω_i. When four of these parameters are specified, equation (3.14) can be solved for the remaining two parameters. For the case of temporal stability, α and β are assumed to be real and fixed, and equation (3.14) provides $\omega = \omega_r + i\omega_i$. Thus, it follows from equation (3.2) that the temporal growth rate is ω_i. For the case of spatial stability, ω is assumed to be real and fixed, and equation (3.14) provides two relations among the remaining four parameters α_r, α_i, β_r, and β_i. The parameters α_r and β_r define a real wavenumber vector $\vec{k}$ whose magnitude k is given by

$$k = (\alpha_r^2 + \beta_r^2)^{\frac{1}{2}}$$

(3.15a)

and whose direction (wave angle) ψ is given by

$$\psi = \arctan (\beta_r / \alpha_r)$$

(3.15b)

Moreover, the parameters α_i and β_i define a growth vector $\vec{\sigma}$ whose magnitude σ is given by

$$\sigma = (\alpha_i^2 + \beta_i^2)^{\frac{1}{2}}$$

(3.15c)

and whose direction (growth direction) $\tilde{\psi}$ is given by

$$\tilde{\psi} = \arctan (\beta_i / \alpha_i)$$

(3.15d)

In general, the growth and wave directions need not coincide and two more relations need to be specified to complete the formulation of the spatial stability problem. Using the method of multiple scales (refs. 37,38), Nayfeh (refs. 21,39) found that the ratio of the group velocity components must be real, thereby providing a third relation. Maximizing the total growth rate can provide the fourth needed relation. These points are discussed further in Section 4. Nayfeh and Padhye (ref. 40) used the complex group velocity vector to relate the problems of temporal and spatial stabilities.

In the case of 2D spatial stability, the two additional relations are given by $\beta = \beta_r + i\beta_i = 0$ and Eq. (3.14) can be used to determine the complex parameter α for any given ω. For the case of 3D spatial stability in boundary layers that depend on x and y only (such as 2D mean flows and flows over an infinite span swept wing), the analysis in Section 4 shows that β = constant and hence Eq. (3.14) can be used to determine the complex parameter α for any given ω and β. In this case, the growth direction is often taken in the x-direction (i.e., β_i is assumed to be zero).

To account for the slow growth of the boundary layer, one can improve the parallel-flow assumption by calculating the local stability of the mean-flow profiles, thereby obtaining values for α and β that vary slowly with x and z. Thus, equation (3.2) is replaced with

$$[u,v,p,T,w] = [\zeta_1(y), \zeta_3(y), \zeta_4(y), \zeta_5(y), \zeta_7(y)] \exp(i\theta)$$

(3.16)

637

where

$$\frac{\partial \theta}{\partial x} = \alpha(x,z), \quad \frac{\partial \theta}{\partial z} = \beta(x,z), \quad \frac{\partial \theta}{\partial t} = -\omega \tag{3.17}$$

and the ζ_n are governed by the eigenvalue problem consisting of equations (3.3)-(3.9). This is the so-called quasi-parallel assumption. As discussed earlier, the growth rate vector is given by

$$\vec{\sigma} = \alpha_i \vec{i} + \beta_i \vec{j}$$

It is independent of the transverse direction and the flow variable whose growth is investigated; neither of these statements is valid for the case of growing boundary layers as discussed in Section 4.

3.1 Inviscid Case

In contrast with the case of incompressible boundary layers, compressible boundary layers, even on flat plates, have inviscid instability, which increases with increasing Mach number. The inviscid instability is governed by equations (3.3)-(3.9) with R being set equal to infinity; that is, it is governed by

$$D\zeta_3 + i\alpha\zeta_1 - \frac{DT_m}{T_m}\zeta_3 + i(\alpha U_m + \beta W_m - \omega)(\gamma M_\infty^2 \zeta_4 - \frac{\zeta_5}{T_m}) + i\beta\zeta_7 = 0 \tag{3.18}$$

$$i(\alpha U_m + \beta W_m - \omega)\zeta_1 + \zeta_3 DU_m + i\alpha T_m \zeta_4 = 0 \tag{3.19}$$

$$i(\alpha U_m + \beta W_m - \omega)\zeta_3 + T_m D\zeta_4 = 0 \tag{3.20}$$

$$i(\alpha U_m + \beta W_m - \omega)\zeta_7 + \zeta_3 DW_m + i\beta T_m \zeta_4 = 0 \tag{3.21}$$

$$i(\alpha U_m + \beta W_m - \omega)\zeta_5 + \zeta_3 DT_m - i(\gamma - 1)T_m M_\infty^2 (\alpha U_m + \beta W_m - \omega)\zeta_4 = 0 \tag{3.22}$$

$$\zeta_3 = \zeta_5 = 0 \quad \text{at} \quad y = 0 \tag{3.23}$$

$$\zeta_n \text{ are bounded as } y \to \infty \tag{3.24}$$

Equations (3.18)-(3.27) can be combined into a second-order equation governing ζ_3 or ζ_4. To accomplish this, we use the transformation (3.10) and (3.11). Thus, we add α times equations (3.19) to β times equation (3.21) and obtain

$$ik(\alpha U_m + \beta W_m - \omega)\eta_1 + \zeta_3 D(\alpha U_m + \beta W_m) + ik^2 T_m \zeta_4 = 0 \tag{3.25}$$

Using equation (3.22) to eliminate ζ_5 from equation (3.18) and using equation (3.10), we obtain

638

$$ikn_1 + D\zeta_3 + iM_\infty^2 (\alpha U_m + \beta W_m - \omega)\zeta_4 = 0 \tag{3.26}$$

Eliminating n_1 from equations (3.25) and (3.26) yields

$$(\alpha U_m + \beta W_m - \omega)D\zeta_3 - \zeta_3 D(\alpha U_m + \beta W_m) = ik^2 T_m(1 - M_r^2)\zeta_4 \tag{3.27}$$

or

$$D\chi = \frac{i(1-M_r^2)M_\infty^2}{M_r^2} \zeta_4 \tag{3.28}$$

where

$$\chi = \frac{\zeta_3}{\alpha U_m + \beta W_m - \omega} \tag{3.29}$$

and

$$M_r = \frac{(\alpha U_m + \beta W_m - \omega)M_\infty}{k\sqrt{T_m}} \tag{3.30}$$

can be interpreted as the local Mach number of the mean flow in the direction of the wavenumber vector $\vec{k} = \alpha\vec{i} + \beta\vec{j}$ relative to the phase velocity ω/k. In general M_r is complex and it is only real for neutral disturbances. In terms of χ and M_r, equation (3.20) can be rewritten as

$$D\zeta_4 = - \frac{ik^2 M_r^2}{M_\infty^2} \chi \tag{3.31}$$

Eliminating ζ_4 from equations (3.28) and (3.31) yields the following second-order equation governing χ:

$$D^2\chi + D\left[\ln \frac{M_r^2}{1-M_r^2}\right]D\chi - k^2(1 - M_r^2)\chi = 0 \tag{3.32}$$

Eliminating χ from equations (3.28) and (3.31) yields

$$D^2\zeta_4 - D(\ln M_r^2)D\zeta_4 - k^2(1 - M_r^2)\zeta_4 = 0 \tag{3.33}$$

In the freestream, $T_m = 1$, $U_m = 1$ and $W_m = 0$ are constants and hence $M_r = M_f$ is a constant and equations (3.32) and (3.33) reduce to

$$D^2\chi - k^2(1 - M_f^2)\chi = 0 \tag{3.34}$$

and

$$D^2\zeta_4 - k^2(1 - M_f^2)\zeta_4 = 0 \tag{3.35}$$

It is clear from equations (3.34) and (3.35) that neutral disturbances decay in the freestream if and only if $M_f^2 < 1$; these disturbances are termed subsonic waves. When $M_f^2 > 1$, neutral disturbances do not vanish in the freestream and they represent

sound waves or Mach waves of the relative flow; they are termed supersonic waves and may be outgoing or incoming waves. When $M_f^2 = 1$, disturbances are termed sonic waves. The above classification is due to Lees and Lin (ref. 2).

For the case of two-dimensional inviscid waves in a two-dimensional boundary layer, Lees and Lin (ref. 2) established a number of conclusions for the case of temporal waves. Their main conclusions are

(i) The necessary and sufficient condition for the existence of a neutral subsonic wave is the presence of a generalized inflection point $y_s > y_0$ in the boundary layer at which

$$D(\rho_m DU_m) = 0 \tag{3.36}$$

where

$$U_m(y_0) = 1 - \frac{1}{M_\infty} \tag{3.37}$$

The phase velocity $c_s = \omega/\alpha_s$ of this neutral wave is $U_m(y_s)$, the mean velocity at the generalized inflection point y_s, which is larger than $1 - \frac{1}{M_\infty}$.

(ii) A sufficient condition for the existence of an unstable subsonic wave is the presence of a generalized inflection point at $y_s > y_0$; its phase velocity $c > 1 - 1/M_\infty$. Compressible boundary-layer flows over insulated flat plates always have inflection points and hence they are unstable to inviscid disturbances.

(iii) There is a neutral subsonic wave having the wavenumber $\alpha = 0$ and the phase velocity $c = c_0$.

(iv) When $M_r^2 < 1$ everywhere in the boundary layer, there is a unique wavenumber α_s corresponding to the phase velocity c_s for the neutral subsonic wave.

Using extensive numerical calculations, Mack (refs. 11,15) established the existence of an infinite sequence of discrete wave numbers α_{sn}, corresponding to an infinite sequence of discrete modes when $M_r^2 > 1$ somewhere in the boundary layer. He referred to the modes that are additional to the mode found by Lees and Lin as higher modes. In contrast with the first mode whose existence depends on the presence of a generalized inflection point, the higher modes exist whenever $M_r^2 > 1$, irrespective of the presence or absence of a generalized inflection point. The lowest Mach number at which the higher modes exist in the boundary layer on an insulated flat plate is 2.2. It turns out that this is also the lowest Mach number at which subsonic higher-mode disturbances exist. The lowest of the subsonic modes is called the second mode and it is the most amplified of the higher modes.

Later, Mack developed a simple theory that provides an approximation to the infinite sequence of wave numbers α_{sn}. He neglected the second term in (3.32) and expressed the solution of the resulting equation that satisfies the boundary condition $v(0)$ as

$$\chi \approx \pm \sin\left[k_{sn} \int_0^y \sqrt{M_r^2 - 1} \, dy\right], \quad y < y_a \tag{3.38}$$

and the solution that decays as $y \to \infty$ as

$$\chi \approx - i \exp\left[- k_{sn} \int_{y_a}^{y} \sqrt{1 - M_r^2} \, dy\right], \quad y > y_a \qquad (3.39)$$

where y_a is the value of y where $M^2 = 1$. He chose the constant in (3.39) to be $-i$ so that the pressure is real and positive for $y > y_a$. He argued that $D\chi$ must go to zero as $y \to y_a$ because the pressure is continuous and finite at $y = y_a$, thereby obtaining the eigenvalues

$$k_{sn} \int_{o}^{y_a} \sqrt{M_r^2 - 1} \, dy = (n - \tfrac{1}{2})\pi, \quad n = 1, 2, 3, \ldots \qquad (3.40)$$

We note that the second term in equation (3.32) is singular at y_a and hence the expansions (3.38) and (3.39) are invalid at $y = y_a$. To connect these expansions, one needs to consider the neighborhood of $y = y_a$, determine an expansion there, and match it to both (3.38) and (3.39). Alternatively, the Langer transformation can be used to determine a single uniformly valid expansion. Even such a consistent expansion is valid only when M_r does not vanish anywhere, (i.e., there is no critical layer) and hence there is no generalized inflection point; otherwise, one cannot neglect the second terms in (3.32) and (3.33). An expansion valid when M_r vanishes somewhere is determined below using the Olver transformation. Mack (refs. 11,15) called the waves when $M_r = 0$ inflectional neutral waves and those which occur when $M_r \neq 0$ non-inflectional neutral waves. His numerical results for the case of non-inflectional neutral waves (Figs. 1 and 2) are qualitatively in agreement with his simple theory, whereas his calculations for the case of inflectional waves (Figs. 3 and 4) differ from those obtained from his simple theory. According to his theory, $\zeta_4(\delta)$ is positive for all modes, there are no zeros in the interval $y > y_a$, and the number of zeros in $y < y_a$ increases by one for each successive mode.

To determine a single uniformly valid expansion, we eliminate the second term in equation (3.33) using the transformation

$$\zeta_4 = M_r \phi \qquad (3.41)$$

and obtain

$$\phi'' - \left[k^2(1 - M_r^2) - \frac{M_r''}{M_r} + \frac{2M_r'^2}{M_r^2}\right]\phi = 0 \qquad (3.42)$$

For the case of non-inflectional waves (i.e., $M_r \neq 0$ everywhere), we use the Langer transformation (refs. 37,38) and obtain the approximate solution

$$\phi \approx \frac{\xi^{1/4}}{\sqrt[4]{1-M_r^2}} \left[c_1 Ai(\xi) + c_2 Bi(\xi)\right] \qquad (3.43)$$

and hence

$$\zeta_4 \approx \frac{M_r \xi^{1/4}}{\sqrt[4]{1-M_r^2}} \left[c_1 Ai(\xi) + c_2 Bi(\xi)\right] \qquad (3.44)$$

where Ai and Bi are the Airy functions of the first and second kind, respectively,

641

$$\frac{2}{3} \xi^{3/2} = k \int_{y_a}^{y} \sqrt{1 - M_r^2} \; dy \tag{3.45}$$

and $y = y_a$ is the turning point at which $M_r^2(y_a) = 1$. Since

$$Ai(\xi) \sim \frac{\exp\left[-\frac{2}{3} \xi^{2/3}\right]}{2\sqrt{\pi} \; \xi^{1/4}} \quad \text{as} \quad \xi \to \infty \tag{3.46}$$

and

$$Bi(\xi) \sim \frac{\exp\left[\frac{2}{3} \xi^{3/2}\right]}{\sqrt{\pi} \; \xi^{1/4}} \quad \text{as} \quad \xi \to \infty \tag{3.47}$$

the vanishing of the disturbance as $y \to \infty$ demands that $c_2 = 0$. Then, the boundary condition $v(0) = 0$ or $\zeta_3(0) = 0$ demands that

$$Ai' = 0 \quad \text{at} \quad y = 0 \tag{3.48}$$

But

$$Ai(\xi) \sim \frac{1}{\sqrt{\pi} \; (-\xi)^{1/4}} \sin\left[\frac{2}{3} (-\xi)^{3/2} + \frac{1}{4} \pi\right] \quad \text{as} \quad \xi \to -\infty \tag{3.49}$$

Hence

$$\cos\left[k \int_{0}^{y_a} \sqrt{M_r^2 - 1} \; dy + \frac{1}{4} \pi\right] = 0 \tag{3.50}$$

Consequently,

$$k_{sn} \int_{0}^{y_a} \sqrt{M_r^2 - 1} \; dy = \left(n - \frac{3}{4}\right)\pi, \quad n = 1, 2, 3, \ldots \tag{3.51}$$

whose righthand side differs from that of Mack by $\frac{1}{4} \pi$. Moreover, the eigenfunction (3.44) with $c_2 = 0$ differs from that of Mack in the presence of the factor $M_r / \sqrt[4]{1 - M_r^2}$ and the phase $\frac{1}{4} \pi$ in the interval $y < y_a$.

For the case of inflectional waves (i.e., $M_r = 0$ at $y = y_c$, $y_c > y_a$), the expansion (3.43) is not valid as $y \to y_c$ and we need an expansion that is valid in the neighborhood of $y = y_c$. Using the Olver transformation (ref. 37), we find that

$$\phi \sim \frac{\left[\int_{y_c}^{y} \sqrt{1-M_r^2} \; dy\right]^{\frac{1}{2}}}{\sqrt[4]{1-M_r^2}} \left\{b_1 I_{3/2}\left[k \int_{y_c}^{y} \sqrt{1 - M_r^2} \; dy\right]\right.$$

$$\left. + b_2 K_{3/2}\left[k \int_{y_c}^{y} \sqrt{1 - M_r^2} \; dy\right]\right\} \tag{3.52}$$

642

which is valid in the interval $y > y_a$. Since

$$I_{3/2}(\xi) \to \frac{1}{\sqrt{2\pi\xi}} \ e^{\xi} \ \text{ and } \ K_{3/2}(\xi) \to \sqrt{\frac{\pi}{2\xi}} \ e^{-\xi} \ \text{ as } \ \xi \to \infty \tag{3.53}$$

the boundary condition that ζ_4 tends to zero as $y \to \infty$ demands that $b_1 = 0$. This expansion needs to be matched with the expansion (3.43) that is valid at the turning point y_a. Expanding (3.43) for large k and for $y > y_a$, expanding (3.52) for large k and for $y < y_c$, means that $b_1 = 0$, we obtain

$$\sqrt{\frac{\pi}{2k}} \ b_2 e^{k\int_y^{y_c}\sqrt{1-M_r^2}dy} = \frac{c_1}{2\sqrt{\pi}} \ e^{-k\int_{y_a}^{y}\sqrt{1-M_r^2}dy} + \frac{c_2}{\sqrt{\pi}} \ e^{-k\int_{y_a}^{y}\sqrt{1-M_r^2}dy} \tag{3.54}$$

Hence, $c_2 = 0$ and

$$b_2 = \frac{c_1\sqrt{k}}{\pi\sqrt{2}} \exp\left[-\int_{y_a}^{y_c}\sqrt{1 - M_r^2} \ dy\right] \tag{3.55}$$

Imposing the boundary condition at the wall that $v(0) = 0$ or $\zeta_3(0) = 0$ yields the eigenvalues as in (3.51). Thus, the difference between inflectional and non-inflectional waves is in the shape of the eigenfunction.

Using extensive numerical computations, Mack established a number of conclusions regarding supersonic stability:

(i) In contrast with incompressible stability theory, there is more than one mode of instability and it is one of the additional modes that is the most unstable. Figure 5 shows the variation of the maximum temporal amplification rate of 2D waves with Mach number. It is clear that below $M_\infty = 2.2$, the boundary layer on an insulated flat plate is virtually stable to inviscid 2D waves and that above $M_\infty = 2.2$ the second mode is the most unstable mode. Moreover, the maximum amplification rate increases sharply as M_∞ increases beyond 2.2. Furthermore, above $M_\infty = 5$, the first mode is not even the second most unstable mode.

(ii) In contrast with incompressible stability theory, 3D first modes are more unstable than their corresponding 2D waves. However, 3D second modes are more stable than their corresponding 2D waves. Figure 6 shows the variation of the temporal amplification rate of the first and second modes with frequency for $M_\infty = 4.5$ and several wave angles. It clearly shows that the most unstable first-mode wave has a wave angle that is approximately 60° and an amplification rate that is approximately twice the maximum amplification rate of its corresponding 2D wave.

(iii) Whereas cooling can stabilize first-mode waves in accordance with the prediction of Lees (ref. 3), cooling destablizes second-mode waves. Figure 7 shows the variation of the maximum temporal growth rate of the first mode at $M_\infty = 3.0$, 4.5, and 5.8 and the second mode at $M_\infty = 5.8$ with the ratio of the wall temperature T_w to the recovery temperature T_r. It is clear that 2D and 3D first-mode waves can be completely stabilized by cooling, whereas second-mode waves are destablished by cooling.

3.2 Viscous Stability for Flat Plates

Again, using extensive numerical calculations, Mack (refs. 10,11) investigated the influence of Mach number on the viscous instability of supersonic flows past flat plates. He found that viscosity is stabilizing for both 2D and 3D first-mode waves when $M_\infty \geq 3.0$ and for second-mode waves at all Mach numbers; that is, the maximum amplification rate (over all frequencies, and wave angles in case of 3D waves, at constant Reynolds number) decreases with decreasing Reynolds number. This result was disputed by Wazzan, Taghavi, and Keltner (ref. 41) who did not find a transition from viscous to inviscid instability with increasing Mach number but found that viscous instability persists to $M = 6.0$. Mack (ref. 42) reconfirmed his calculations for the case of temporal stability and obtained spatial stability results that agree with his earlier conclusions on the influence of viscosity on compressible stability. Moreover, the spatial stability calculations of El-Hady and Nayfeh (ref. 19) and Nayfeh and Harper (ref. 43) agree with those of Mack for at least three significant figures for all the calculations they performed. Moreover, the calculations of Malik qualitatively agree with those of Mack.

Figure 8 shows the neutral stability curves of 2D waves calculated by Mack at $M_\infty = 1.6$, 2.2, 2.6, 3.0, and 3.8. He plotted α vs. R^{-1} to emphasize the higher Reynolds number region. Comparing the neutral curve for $M_\infty = 1.6$ with that of the Blasius flow (i.e., $M_\infty = 0$) shows that, although they have the same general type, compressiblity drastically reduced the viscous instability, resulting in much lower neutral wave numbers. As the Mach number increases beyond 1.6, the viscous instability continues to weaken although the effect of the increase in inviscid instability continues to extend to lower and lower Reynolds numbers. When M_∞ reaches 3.8, the viscous instability disappears and viscosity acts only to damp out the inviscid instability.

As in the case of inviscid instability, the most unstable first-mode waves are 3D waves. Figure 9 shows the variation of the maximum temporal amplification rate of 2D and 3D waves with Reynolds number for $M_\infty = 1.3$, 1.6, 2.2, and 3.0 and Figure 10 shows the variation of the maximum spatial amplification rate of 2D and 3D waves at $\psi = 50°$ with R for $M_\infty = 1.6$ (ref. 19). The most unstable wave angles of 3D waves are shown in Figure 9. At $M_\infty = 1.3$, the instability of 2D and 3D waves is due to viscosity. As M_∞ increases, the viscous instability decreases for both 2D and 3D waves. Whereas increasing the Mach number results in a drastic decrease in the 2D maximum growth rates, it produces only a slight change in those of the 3D waves.

As in the inviscid case, the numerical results of Mack suggest that the 2D second- and higher-mode waves are more unstable than their corresponding 3D waves. Moreover, the maximum growth rate of second-mode waves drops sharply as the wave angle increases from zero.

The lowest Mach number at which Mack was able to calculate 2D second-mode waves is $M_\infty = 3.0$ at which the minimum critical Reynolds number is 13,900. As pointed out in the preceding section, the inviscid instability increases rapidly with increasing Mach number and hence one would expect the minimum critical Reynolds number to decrease rapidly to lower values as the Mach number decreases. In fact, Mack found that the minimum critical Reynolds numbers drops to 235 as the Mach number increases to 4.5. Moreover, at high Mach numbers second-mode waves have much higher growth rates than oblique first-mode waves.

Whereas cooling can stabilize 2D and 3D first-mode waves, second-mode waves cannot be stabilized by cooling. On the contrary second-mode waves are destabilized

by cooling. Malik (ref. 43) studied the influence of cooling on oblique first-mode waves at $\psi = 60°$ for $M_\infty = 2$ and 4.5 and second-mode waves for $M_\infty = 4.5$; in these calculations $R = 1500$ and the stagnation temperature is $560°R$. Figure 11 shows that the oblique first-mode wave at $M = 2$ is completely stabilized when $T_w/T_{ad} = 0.7$, whereas that at $M_\infty = 4.5$ is stabilized only when $T_w/T_{ad} = 0.48$. On the other hand, Figs. 11 and 12 show that the second-mode wave is destablished by cooling. In fact, the maximum growth rate increases rapidly with cooling. Malik found that the frequency of most amplified first-mode wave decreases with cooling whereas that of the most amplified second-mode wave increases with cooling.

Malik (ref. 43) also investigated the influence of favorable pressure gradients (Fig. 13) and suction (Fig. 14) on the stabilization of second-mode waves. He found that each of them shifts the band of unstable frequencies to higher values and reduces the peak amplification. Consequently, it appears that, whereas cooling cannot be used to stabilize second-mode waves, they can be stablized using either suction or wall shaping to produce a favorable pressure gradient.

Preliminary results of Malik (ref. 43) indicate that real gas effects tend to destabilize hypersonic boundary layers.

4. NONPARALLEL STABILITY

We confine our consideration to mean flows that are slightly nonparallel, that is, the normal velocity component V_m is small compared with the other components U_m and W_m. This in turn implies that all the mean-flow variables must be weak functions of the streamwise and spanwise coodinates. In other words

$$U_m = U_m(x_1,y,z_1) \ , \ V_m = \epsilon V_m^*(x_1,y,z_1), \ W_m = W_m(x_1,y,z_1) \tag{4.1}$$

$$p_m = p_m(x_1,z_1) \ , \ T_m = T_m(x_1,y,z_1) \tag{4.2}$$

where $V_m^* = O(1)$. We describe the relatively slow variations of the mean-flow quantities in the streamwise and spanwise directions by the slow scales $x_1 = \epsilon x$ and $z_1 = \epsilon z$, respectively, where $\epsilon = 1/R$.

We use the method of multiple scales (refs. 37,38) to determine a uniformly valid asymptotic expansion of the solution of equations (2.3)-(2.9), (2.12) and (2.13) in the form

$$q(x,y,z,t;\epsilon) = \left[q_0(x_1,y,z_1,t_1) + \epsilon q_1(x_1,y,z_1,t_1) + \ldots \right] \exp(i\theta) \tag{4.3}$$

where $t_1 = \epsilon t$, a slow time scale, and

$$\frac{\partial \theta}{\partial x} = \alpha(x_1,z_1) \ , \ \frac{\partial \theta}{\partial z} = \beta(x_1,z_1) \ , \ \frac{\partial \theta}{\partial t} = -\omega \tag{4.4}$$

Assuming the phase θ to be twice continuously differentiable, we have

$$\frac{\partial \alpha}{\partial z_1} = \frac{\partial \beta}{\partial x_1} \tag{4.5}$$

In the case of mean flows that are independent of z, such as 2D mean flows and flows over infinite-span swept wings, $\alpha = \alpha(x_1)$ and $\beta = \beta(x_1)$, because the coefficients of equations (2.3)-(2.9) are independent of z_1. Then, it follows from equation (4.5) that β = constant. Substituting equations (4.1)-(4.4) into equations (2.3)-(2.9), (2.12) and (2.13) and equating coefficients of like powers of ε, we obtain problems describing the zeroth- and first-order disturbances.

4.1 Zeroth-Order Problem

$$L_1(u_0,v_0,w_0,p_0,T_0) = - i\rho_m(\omega - \alpha U_m - \beta W_m)\left(\frac{p_0}{p_m} - \frac{T_0}{T_m}\right) + i\rho_m(\alpha u_0 + \beta w_0)$$

$$+ D(\rho_m v_0) = 0 \tag{4.6}$$

$$L_2(u_0,v_0,w_0,p_0,T_0) = - i\rho_m(\omega - \alpha U_m - \beta W_m)u_0 + \rho_m v_0 DU_m + i\alpha p_0$$

$$- \frac{1}{R}\left\{- \mu_m(r\alpha^2 + \beta^2)u_0 + D(\mu_m Du_0) + i\alpha\mu_m(1 + m)Dv_0\right.$$

$$+ i\alpha v_0 D\mu_m - \alpha\beta\mu_m(1 + m)w_0 + D\left(\frac{d\mu_m}{dT} T_0\right)DU_m + \frac{d\mu_m}{dT} T_0 D^2 U_m\left.\right\} = 0$$

$$\tag{4.7}$$

$$L_3(u_0,v_0 \cdot w_0,p_0,T_0) = - i\rho_m(\omega - \alpha U_m - \beta W_m)v_0 + Dp_0$$

$$- \frac{1}{R}\left\{i\mu_m(1 + m)(\alpha Du_0 + \beta Dw_0) + im(\alpha u_0 + \beta w_0)D\mu_m\right.$$

$$- (\alpha^2 + \beta^2)\mu_m v_0 + D(\mu_m rDv_0) + i(\alpha DU_m + \beta DW_m)\frac{d\mu_m}{dT} T_0\left.\right\} = 0$$

$$\tag{4.8}$$

$$L_4(u_0,v_0,w_0,p_0,T_0) = - i\rho_m(\omega - \alpha U_m - \beta W_m)w_0 + \rho_m v_0 DW_m + i\beta p_0$$

$$- \frac{1}{R}\left\{- \alpha\beta\mu_m(1 + m)u_0 + i\beta\mu_m(1 + m)Dv_0 + i\beta v_0 D\mu_m\right.$$

$$- \mu_m(\alpha^2 + r\beta^2)w_0 + D(\mu_m Dw_0) + D\left(\frac{d\mu_m}{dT} T_0\right)DW_m + \frac{d\mu_m}{dT} T_0 D^2 W_m\left.\right\} = 0$$

$$\tag{4.9}$$

$$L_5(u_0, v_0, w_0, p_0, T_0) = -i\rho_m(\omega - \alpha U_m - \beta W_m)T_0 + \rho_m v_0 DT_m + i(\gamma - 1)M_\infty^2 p_0$$

$$\cdot (\omega - \alpha U_m - \beta W_m) - \frac{(\gamma - 1)M_\infty^2}{R}\{2\mu_m(DU_m Du_0 + DW_m Dw_0)$$

$$+ 2i\mu_m(\alpha DU_m + \beta DW_m)v_0 + \frac{d\mu_m}{dT}[(DU_m)^2 + (DW_m)^2]T_0\}$$

$$- \frac{1}{RPr}\{2D\mu_m DT_0 + \mu_m D^2 T_0 - (\alpha^2 + \beta^2)\mu_m T_0 + D^2\mu_m T_0\} = 0 \tag{4.10}$$

$$u_0 = v_0 = w_0 = T_0 = 0 \quad \text{at} \quad y = 0 \tag{4.11}$$

$$u_0, v_0, w_0, T_0 \rightarrow 0 \quad \text{as} \quad y \rightarrow \infty \tag{4.12}$$

The solution of the zeroth-order problem can be expressed as

$$[u_0, Du_0, v_0, T_0, DT_0, w_0, Dw_0]^T = A(x_1, z_1, t_1)\zeta(x_1, z_1, y) \tag{4.13}$$

where ζ is a column vector having 8 components and is governed by the quasi-parallel eigenvalue problem (3.13). The function $A(x_1, z_1, t_1)$ is arbitrary at this level of approximation; it will be determined by imposing the solvability condition at the next level of approximation.

4.2 First-Order Problem

Using equation (4.13), we write the first-order problem as

$$Dz_{1n} - \sum_{m=1}^{8} a_{nm}z_{1m} = D_n\frac{\partial A}{\partial t_1} + E_n\frac{\partial A}{\partial x_1} + F_n\frac{\partial A}{\partial z_1} + G_n A \tag{4.14}$$

$$z_{11} = z_{13} = z_{17} = 0, \ z_{15} = 0 \quad \text{at} \quad y = 0 \tag{4.15}$$

$$z_{1n} \text{ is bounded as } y \rightarrow \infty \tag{4.16}$$

where

$$z_{11} = u_1, \ z_{12} = Du_1, \ z_{13} = v_1, \ z_{14} = p_1 \tag{4.17}$$

$$z_{15} = T_1, \ z_{16} = DT_1, \ z_{17} = w_1, \ z_{18} = Dw_1 \tag{4.18}$$

and the D_n, E_n, F_n, and G_n are known functions of the ζ_n, α, β, and the mean-flow quantities; they are defined in Appendix B. Since the homogeneous problem (4.14)-(4.16) has a nontrivial solution, the inhomogeneous problem has a solution only if

the right-hand side of equation (4.14) is orthogonal to every solution of the adjoint homogeneous problem (ref. 38)

$$D\zeta_n^* + \sum_{m=1}^{8} a_{mn}\zeta_m^* = 0 \tag{4.19}$$

$$\zeta_2^* = \zeta_4^* = \zeta_8^* = 0, \quad \zeta_6^* = 0 \quad \text{at} \quad y = 0 \tag{4.20}$$

$$\zeta_n^* \text{ is bounded as } y \to \infty \tag{4.21}$$

The solvability condition takes the form

$$\int_0^\infty \sum_{n=1}^{8} \left[D_n \frac{\partial A}{\partial t_1} + E_n \frac{\partial A}{\partial x_1} + F_n \frac{\partial A}{\partial z_1} + G_n A \right] \zeta_n^* dy = 0 \tag{4.22}$$

Substituting for the D_n, E_n, F_n, and G_n from Appendix B into equation (4.22) yields the following partial-differential equation governing the modulation of A:

$$\frac{\partial A}{\partial t} + \omega_\alpha \frac{\partial A}{\partial x} + \omega_\beta \frac{\partial A}{\partial z} = \epsilon h_1(\alpha,\beta,x,z)A \tag{4.23}$$

where ω_α and ω_β are the group velocity components in the x and z directions; they, along with h_1, are given in quadratures, as in Appendix C.

Equation (4.23) shows that A is a function of x and z as well as α and β. To determine the equations describing α and β, we differentiate equations (3.13) with respect to x_1 and obtain

$$D\left(\frac{\partial \zeta_n}{\partial x_1}\right) - \sum_{m=1}^{8} a_{nm}\left(\frac{\partial \zeta_m}{\partial x_1}\right) = iE_n \frac{\partial \alpha}{\partial x_1} + iF_n \frac{\partial \beta}{\partial x_1} + \sum_{m=1}^{8} \frac{\partial a_{mn}}{\partial x_1}\bigg|_{\alpha,\beta} \zeta_m \tag{4.24}$$

$$\frac{\partial \zeta_1}{\partial x_1} = \frac{\partial \zeta_3}{\partial x_1} = \frac{\partial \zeta_5}{\partial x_1} = \frac{\partial \zeta_7}{\partial x_1} = 0 \quad \text{at} \quad y = 0 \tag{4.25}$$

$$\frac{\partial \zeta_n}{\partial x_1} \text{ is bounded as } y \to \infty \tag{4.26}$$

Imposing the solvability condition on equations (4.24)-(4.26) yields

$$\omega_\alpha \frac{\partial \alpha}{\partial x_1} + \omega_\beta \frac{\partial \beta}{\partial x_1} = h_2(\alpha,\beta,x_1,z_1) \tag{4.27}$$

where h_2 is defined in Appendix C. Similarly, differentiating equations (3.13) with respect to z_1 and imposing the solvability condition for the resulting problem, we obtain

$$\omega_\alpha \frac{\partial \alpha}{\partial z_1} + \omega_\beta \frac{\partial \beta}{\partial z_1} = h_3(\alpha,\beta,x_1,z_1) \tag{4.28}$$

where h_3 is defined in Appendix C. Using equation (4.5), we rewrite equations (4.27) and (4.28) as

$$\omega_\alpha \frac{\partial \alpha}{\partial x} + \omega_\beta \frac{\partial \alpha}{\partial z} = \epsilon h_2 \tag{4.29}$$

$$\omega_\alpha \frac{\partial \beta}{\partial x} + \omega_\beta \frac{\partial \beta}{\partial z} = \epsilon h_3 \tag{4.30}$$

Therefore, equations (4.23), (4.29), and (4.30) describe the modulation of A, α, and β with x, z, and t.

For a monochromatic wave, $\partial A/\partial t = 0$ and equation (4.23) reduces to

$$\omega_\alpha \frac{\partial A}{\partial x} + \omega_\beta \frac{\partial A}{\partial z} = \epsilon h_1 A \tag{4.31}$$

Nayfeh (ref. 21) argued that, in general, $\omega_\beta/\omega_\alpha$ is complex and hence equation (4.31) is elliptic for real x and z. In order that equation (4.31) be hyperbolic representing a propagating wave, $\omega_\beta/\omega_\alpha$ must be real and equations (4.29)-(4.31) reduce to the ordinary differential equations

$$\frac{dA}{ds} = \frac{\epsilon h_1 A}{\omega_\alpha}, \quad \frac{d\alpha}{ds} = \frac{\epsilon h_2}{\omega_\alpha}, \quad \frac{d\beta}{ds} = \frac{\epsilon h_3}{\omega_\alpha} \tag{4.32}$$

along the characteristic

$$\frac{dx}{ds} = 1 \quad \text{and} \quad \frac{dz}{ds} = \frac{\omega_\beta}{\omega_\alpha} \tag{4.33}$$

Thus,

$$A = A_0 \exp\left[\epsilon \int (h_1/\omega_\alpha) ds\right] = A_0 \exp\left[\epsilon \int (h_1/\omega_\alpha) dx\right] \tag{4.34}$$

and

$$\alpha = \epsilon \int h_2 ds, \quad \beta = \epsilon \int h_3 ds \tag{4.35}$$

where A_0 is a constant. Therefore, to the first approximation,

$$u \approx A_0 \zeta_1(x,y,z) \exp\left[i\int (\alpha + \beta \frac{\omega_\beta}{\omega_\alpha}) dx + \epsilon \int \frac{h_1}{\omega_\alpha} dx - i\omega t\right] \tag{4.36}$$

For the case of parallel flows, the condition $\omega_\beta/\omega_\alpha$ be real reduces to $d\alpha/d\beta$ being real, which was obtained by Nayfeh (ref. 21) and Cebeci and Stewartson (ref. 44) using the saddle-point method.

4.3 Growth Rate

Defining the growth rate in the streamwise direction as

$$\sigma_x = \text{Real}\left[\frac{\partial}{\partial x} (\ln u)\right]$$

we find from equation (4.36) that

$$\sigma_x = -(\alpha_i + \beta_i \frac{\omega_\beta}{\omega_\alpha}) + \varepsilon \text{ Real } (\frac{h_1}{\omega_\alpha}) + \frac{\partial}{\partial x} (\ln\zeta_1) \qquad (4.37)$$

The first term is the quasiparallel contribution and the last two terms are due to the growth of the boundary layer. Whereas the second term is independent of the transverse direction, the third term strongly depends on the transverse direction. Hence, in contrast with the parallel or quasiparallel case, the local growth rate depends on both the streamwise and transverse directions. Moreover, the transverse variation depends on the flow variable being investigated.

It follows from equation (4.36) that the amplification factor is

$$\frac{\zeta_n(x,y,z)}{\zeta_n(x_0,y,z)} \exp[-\int_{x_0}^{x} (\alpha_i + \beta_i \frac{\omega_\beta}{\omega_\alpha})dx + \varepsilon\text{Real} \int_{x_0}^{x} \frac{h_1}{\omega_\alpha} dx] \qquad (4.38)$$

Again, the amplification factor is a function of the transverse location. However, the variation is a simple one. For a detailed discussion of the case of a wave packet, the reader is referred to the article of Nayfeh (ref. 21).

For the case of two-dimensional flows, β is a constant. Then, for the case of monochromatic waves, equation (4.36) reduces to

$$u \approx A_0\zeta_1(x,y)\exp[i(\int\alpha dx + \beta z - \omega t) + \varepsilon\int \frac{h_1}{\omega_\alpha} dx] \qquad (4.39)$$

Consequently, the growth direction is the streamwise direction and the growth rate

$$\sigma = \text{Real}[\frac{\partial}{\partial x}(\ln u)]$$

is given by

$$\sigma = -\alpha_i + \varepsilon\text{Real}(\frac{h_1}{\omega_\alpha}) + \text{Real}[\frac{\partial}{\partial x}(\ln\zeta_1)] \qquad (4.40)$$

Since ζ_1 is a function of y and, in general, distorts with the streamwise distance, one may term stable disturbances unstable and vice versa. Because of the mode-shape distortion, neutral stability points are a function of both the transverse and streamwise positions. The experiments of Laufer and Vrebalovich (ref. 23) clearly show that the growth of the disturbances and the neutral curves obtained depend on the value of y*/L* at which the observations were made. Moreover, a different growth rate would be obtained if one replaces u with another variable such as v, p, w, or T. On the other hand, for the case of parallel flows, the last two terms in equation (4.40) vanish and the growth rate is unique and independent of the varible being used or the transverse direction at which the growth rate is determined. Therefore, to compare the analytical results with experimental data in growing boundary layers, one needs to make the calculations in the same manner in which the measurements are taken. Available experimental stability studies almost exclusively use hot-wire or hot-film anemometers following disturbances in the boundary layer. The hot-wire or hot-film response is a combination of velocity,

density, and temperature fluctuations. The hot-wire response when operated at high constant overheat is proportional to the rms of the mass-flow fluctuations. To describe fully the disturbance, one needs measurements of all fluctuation characteristics such as the rms amplitude, spectra, wave angle, and propagation speed as functions of x, y, and z. Except for the experiment of Kendall (ref. 25), no information is available on the disturbance waveangle. Laufer and Vrebalovich reported measurements at different constant y*/L*, whereas Kendall, Demetriades, Legiga et al, and Stetson et al reported measurements at one constant y*/L* located in the wideband energy peak. However, available calculations do not agree with each other. Some calculations show large nonparallism influence, whereas other calculations show small influence.

5. SUBHARMONIC INSTABILITY

In this case, the basic flow is taken as the sum of the mean steady flow and a two-dimensional quasiparallel T-S wave; that is

$$u_b = U_m(y) + A[\varsigma_1(y)e^{i\theta} + cc] \tag{5.1}$$

$$v_b = A[\varsigma_3(y)e^{i\theta} + cc] \tag{5.2}$$

$$p_b = p_m + A[\varsigma_4(y)e^{i\theta} + cc] \tag{5.3}$$

$$T_b = T_m(y) + A[\varsigma_5(y)e^{i\theta} + cc] \tag{5.4}$$

$$w_b = 0 \tag{5.5}$$

$$\frac{\partial\theta}{\partial x} = \alpha_r \quad \text{and} \quad \frac{\partial\theta}{\partial t} = -\omega \tag{5.6}$$

where cc stands for the complex conjugate of the preceding terms, α_r and ω are real, and A and α_r are approximated locally by constant values. Substituting equations (5.1)-(5.6) into equations (2.3)-(2.9), (2.12) and (2.13) yields a system of partial differential equations whose coefficients are independent of z, periodic in x and t, and dependent in a complicated manner on y. Consequently, the z-variation can be separated and using Floquet theory, one can represent the solutions of the problem as

$$u = \exp(\sigma_x x + \sigma_t t)\cos\beta z \ \phi_1(x,y,t) \tag{5.7}$$

$$v = \exp(\sigma_x x + \sigma_t t)\cos\beta z \ \phi_3(x,y,t) \tag{5.8}$$

$$p = \exp(\sigma_x x + \sigma_t t)\cos\beta z \ \phi_4(x,y,z) \tag{5.9}$$

$$T = \exp(\sigma_x x + \sigma_t t)\cos\beta z \ \phi_5(x,y,t) \tag{5.10}$$

$$w = \exp(\sigma_x x + \sigma_t t)\sin\beta z \; \phi_7(x,y,t) \tag{5.11}$$

where σ_x and σ_t are called the characteristic exponents and the ϕ_n are periodic in x and t. For the subharmonic parametric case, the ϕ_n have a period that is twice the period of the primary flow and to the first approximation equations (5.7)-(5.11) become

$$u = \exp(\sigma_x x + \sigma_t t)\cos\beta z\left[\xi_1(y)\exp(\tfrac{1}{2}i\theta) + cc\right] \tag{5.12}$$

$$v = \exp(\sigma_x x + \sigma_t t)\cos\beta z\left[\xi_3(y)\exp(\tfrac{1}{2}i\theta) + cc\right] \tag{5.13}$$

$$p = \exp(\sigma_x x + \sigma_t t)\cos\beta z\left[\xi_4(y)\exp(\tfrac{1}{2}i\theta) + cc\right] \tag{5.14}$$

$$T = \exp(\sigma_x x + \sigma_t t)\cos\beta z\left[\xi_5(y)\exp(\tfrac{1}{2}i\theta) + cc\right] \tag{5.15}$$

$$w = \exp(\sigma_x x + \sigma_t t)\sin\beta z\left[\xi_7(y)\exp(\tfrac{1}{2}i\theta) + cc\right] \tag{5.16}$$

For the case of temporal stability $\sigma_x = 0$ and $\sigma_t \neq 0$, whereas for the case of spatial stability $\sigma_t = 0$ and $\sigma_x \neq 0$.

Substituting equations (5.1)-(5.6) and (5.12)-(5.16) into equations (2.3)-(2.9), (2.12) and (2.13) and equating the coefficients of $\exp(\tfrac{1}{2}i\theta)$ on both sides leads to the following problem governing the ξ_n and either σ_x or σ_t (ref. 45):

$$\left[\sigma_t - \tfrac{1}{2}i\omega + (\sigma_x + \tfrac{1}{2}i\alpha_r)U_m\right](\gamma M_\infty^2 \xi_4 - \rho_m\xi_5) + (\sigma_x + \tfrac{1}{2}i\alpha_r)\xi_1$$

$$+ \frac{D\rho_m}{\rho_m}\xi_3 + D\xi_3 + \beta\xi_7 + (\sigma_x + \tfrac{1}{2}i\alpha_r)A(\gamma M_\infty^2\zeta_4 - \rho_m\zeta_5)\bar{\xi}_1$$

$$+ (\sigma_x + \tfrac{1}{2}i\alpha_r)A\zeta_1(\gamma M_\infty^2\bar{\xi}_4 - \rho_m\bar{\xi}_5) + \frac{A}{\rho_m}\frac{\partial}{\partial y}\left[\rho_m(\gamma M_\infty^2\zeta_4 - \rho_m\zeta_5)\bar{\xi}_3\right.$$

$$\left. + \rho_m\zeta_3(\gamma M_\infty^2\bar{\xi}_4 - \rho_m\bar{\xi}_5)\right] + A(\gamma M_\infty^2\zeta_4 - \rho_m\zeta_5)\bar{\xi}_7 = 0 \tag{5.17}$$

$$\left[\sigma_t - \frac{1}{2}i\omega + U_m(\sigma_x + \frac{1}{2}i\alpha_r) - \frac{r\mu_m}{\rho_m R}(\sigma_x + \frac{1}{2}i\alpha_r)^2 + \frac{\mu_m\beta^2}{\rho_m R}\right]\xi_1$$

$$+ \frac{\mu_m'}{\rho_m R}\xi_2 + \left[DU_m - \frac{\mu_m'}{\rho_m R}(\sigma_x + \frac{1}{2}i\alpha_r)\right]\xi_3 + \frac{(\sigma_x + \frac{1}{2}i\alpha_r)}{\rho_m}\xi_4 - \frac{D(\mu_m' DU_m)}{\rho_m R}\xi_5$$

$$- \frac{\mu_m' DU_m}{\rho_m R} - \frac{(m+1)\mu_m\beta}{\rho_m R}(\sigma_x + \frac{1}{2}i\alpha_r)\xi_7 - \frac{(m+1)\mu_m}{\rho_m R}(\sigma_x + \frac{1}{2}i\alpha_r)D\xi_3$$

$$- \frac{\mu_m}{\rho_m R}D\xi_2 + A\{\zeta_1(\sigma_x + \frac{1}{2}i\alpha_r) + [\sigma_t + \frac{1}{2}i\omega + U_m(\sigma_x$$

$$- \frac{1}{2}i\alpha_r)](\gamma M_\infty^2\zeta_4 - \rho_m\zeta_5) - \frac{r\mu_m'\zeta_5}{\rho_m R}(\sigma_x^2 + \frac{1}{4}\alpha_r^2)\}\bar{\xi}_1$$

$$+ A\left[\zeta_3 - \frac{D(\mu_m'\zeta_5)}{\rho_m R}\right]\bar{\xi}_2 + A[D\zeta_1 + DU_m(\gamma M_\infty^2\zeta_4 - \rho_m\zeta_5)$$

$$- \frac{D(\mu_m'\zeta_5)}{\rho_m R}(\sigma_x - \frac{1}{2}i\alpha_r)]\bar{\xi}_3 + A[i(\alpha_r U_m - \omega)\zeta_1$$

$$+ DU_m\zeta_3](\gamma M_\infty^2\bar{\xi}_4 - \rho_m\bar{\xi}_5) - \frac{A}{\rho_m R}\{\mu_m'(i r\alpha_r\zeta_1 + mD\zeta_3)(\sigma_x + \frac{1}{2}i\alpha_r)$$

$$+ \mu_m(D^2\zeta_1 + i\alpha_r D\zeta_3) + D\mu_m'(D\zeta_1 + i\alpha_r\zeta_3)]\bar{\xi}_5 - \frac{A\mu_m'}{\rho_m R}(D\zeta_1$$

$$+ i\alpha_r\zeta_3)\bar{\xi}_6 - \frac{A\beta\mu_m'}{\rho_m R}[m(\sigma_x + \frac{1}{2}i\alpha_r) + (\sigma_x - \frac{1}{2}i\alpha_r)]\bar{\xi}_7 = 0 \qquad (5.18)$$

$$- \frac{2(\gamma-1)M_\infty^2 DU_m}{R\rho_m} \xi_2 + \left[DT_m - \frac{2(\gamma-1)M_\infty^2 DU_m}{\rho_m R}(\sigma_x + \frac{1}{2} i\alpha_r) \right] \xi_3$$

$$- \frac{(\gamma-1)M_\infty^2}{\rho_m} \left[\sigma_t - \frac{1}{2} i\omega + U_m (\sigma_x + \frac{1}{2} i\alpha_r) \right] \xi_4 + \{ \sigma_t - \frac{1}{2} i\omega$$

$$+ U_m (\sigma_x + \frac{1}{2} i\alpha_r) - \frac{(\gamma-1)M_\infty^2 \mu_m'(DU_m)}{R\rho_m} - \frac{1}{\rho_m RPr} \left[\mu_m(\sigma_x + \frac{1}{2} i\alpha_r)^2 \right.$$

$$+ \mu_m' D^2 T_m + D\mu_m' DT_m - \beta^2 \mu_m \}] \xi_5 - \frac{D\mu_m + \mu_m' DT_m}{\rho_m RPr} \xi_6 - \frac{\mu_m}{\rho_m RPr} D\xi_6$$

$$+ A\{ i\alpha_r \zeta_5 - \frac{(\gamma-1)M_\infty^2}{\rho_m} \left[i\alpha_r \zeta_4 + \frac{2m\mu_m}{R} (\sigma_x - \frac{1}{2} i\alpha_r)D\zeta_3 \right.$$

$$+ \frac{2ir\mu_m \alpha_r}{R} (\sigma_x - \frac{1}{2} i\alpha_r)\zeta_1] \} \bar{\xi}_1 - \frac{2A(\gamma-1)M_\infty^2}{R\rho_m} \left[D\zeta_1 + i\alpha_r \zeta_3 \right.$$

$$+ \mu_m' DU_m \zeta_5] \bar{\xi}_2 + A\{ (\gamma M_\infty^2 \zeta_4 - \rho_m \zeta_5)DT_m + D\zeta_5 - \frac{2(\gamma-1)M_\infty^2}{R\rho_m} (\sigma_x - \frac{1}{2} i\alpha_r) [D\zeta_1$$

$$+ i\alpha_r \zeta_3 + \mu_m' \zeta_5 DU_m] \} \bar{\xi}_3 + A\{ \gamma [i(\alpha_r U_m - \omega)\zeta_5 + \zeta_3 DT_m]$$

$$- \frac{(\gamma-1)}{\rho_m}(\sigma_x - \frac{1}{2} i\alpha_r)\zeta_1 \bar{\xi}_4 + A\{ - \gamma M_\infty^2 [i(\alpha_r U_m - \omega)\zeta_5 + \zeta_3 DT_m]$$

$$+ \left[\sigma_t + \frac{1}{2} i\omega + U_m(\sigma_x - \frac{1}{2} i\alpha_r) \right](\gamma M_\infty^2 \zeta_4 - \rho_m \zeta_5) - \frac{2(\gamma-1)M_\infty^2 \mu_m' DU_m}{R\rho_m} (D\zeta_1$$

$$+ i\alpha_r \zeta_3) - \frac{D\mu_m'}{\rho_m RPr} D\zeta_5 - \frac{\mu_m'}{\rho_m RPr} \left[(\sigma_x^2 + \frac{1}{4} \alpha_r^2)\zeta_5 + i\alpha_r(\sigma_x + \frac{1}{2} i\alpha_r)\zeta_5 \right.$$

$$+ D^2 \zeta_5 - \beta^2 \zeta_5] \} \bar{\xi}_5 + A\{ \zeta_3 - \frac{1}{\rho_m RPr} \left[(D(\mu_m' \zeta_5) + \mu_m' D\zeta_5) \right] \} \bar{\xi}_6$$

$$- A \frac{2m(\gamma-1)M_\infty^2 \beta \mu_m}{\rho_m R} (i\alpha_r \zeta_1 + D\zeta_3)\bar{\xi}_7 - A \frac{2(\gamma-1)M_\infty^2 \mu_m}{\rho_m R} (rD\zeta_3 + im\alpha_r \zeta_1)D\bar{\xi}_3$$

$$- \frac{A(\gamma-1)M_\infty^2}{\rho_m} \zeta_3 D\bar{\xi}_4 - \frac{A\mu_m'}{\rho_m RPr} \zeta_5 D\bar{\xi}_6 \qquad\qquad (5.21)$$

$$\xi_1 = \xi_3 = \xi_7 = 0 \quad \text{and} \quad \xi_5 = 0 \quad \text{at} \quad y = 0 \qquad (5.22)$$

$$\xi_n \to 0 \quad \text{as} \quad y \to \infty \qquad (5.23)$$

where

$$\xi_2 = D\xi_1, \quad \xi_6 = D\xi_5, \quad \text{and} \quad \xi_8 = D\xi_7 \qquad (5.24)$$

As an alternative to the collocation technique used by Herbert for the incompressible case (refs. 46,47), Nayfeh and Harper (ref. 45) followed Nayfeh and Masad (ref. 48) and used a shooting technique to solve the eigenvalue problem consisting of equations (5.17)-(5.23) after casting them into a first-order system of equations. The boundary conditions (5.23) at infinity were replaced with boundary conditions at some finite value y_{max} of y outside the boundary layer. Thus, for $y > y_{max}$, $U_m \to 1$ and $DU_m \to 0$. Since the primary eigenfunctions ξ_m decay exponentially outside the boundary layer, Nayfeh and Harper (ref. 45) followed Nayfeh and Masad (ref. 48) and chose a large enough y_{max} so that the ξ_m are very small. The error involved was monitored by choosing a certain value of y_{max}, and solving the problem, then increasing y_{max}, resolving the problem and noting the effect of increasing y_{max} on the accuracy of the solution.

Since no numerical or experimental results are available for compressible flows, Nayfeh and Harper checked the compressible code against the incompressible results of Herbert (refs. 46,47) obtained using a collocation method and those of Nayfeh and Masad (ref. 48) obtained using a shooting technique, which are in good agreement with the experimental results of Kachanov and Levchenko (ref. 49). The agreement is excellent. Next, Nayfeh and Harper produced results to evaluate the influence of compressibility on the secondary instability of first- and second-mode waves.

Letting $R = 1048.8$ and choosing an $F = 83 \times 10^{-6}$, Nayfeh and Harper solved the eigenvalue problem and obtained the 2D T-S waves for $M_\infty = 0.01$, 0.8, and 1.6. These primary waves are stable having the spatial decay rates -0.0216, -0.0166, and -0.0066. Setting the amplitudes of these primary waves at $a = 0.02/\sqrt{2}$, choosing a value for β, and assuming a value for γ_i, they solved the secondary eigenvalue problem and obtained γ_r. Varying γ_i and repeating the calculations, they determined the maximum value of γ_r over all possible values of γ_i. We note that when $M_\infty > 0$ the maximum value of γ_r does not correspond to $\gamma_i = 0$ as in the incompressible case. The results are shown as the dark curves in Figure 15. The growth rates corresponding to $a = 0.01/\sqrt{2}$ are shown as the light curves in Figure 15. Figure 16 shows the growth rates when $a = 0$, that is, the growth rates of the free propagating waves. The results in Figures 15 and 16 show that the secondary growth rates are much larger than the growth rates of the free waves. In fact, for $M_\infty = 1.6$, the free wave is stable for all values of β, whereas the secondary wave is unstable for a very wide range of values of β. Increasing the amplitude of the primary wave results in an increase in the growth rates of all secondary waves. For a given Mach number, the growth rate has a broad maximum. This maximum shifts to larger values of β as the amplitude of the primary wave increases. And for a given amplitude of the primary wave, the maximum growth rate shifts to lower values of β as the Mach number increases.

As discussed in Section 3, as M_∞ increases beyond 3.0, higher-modes become unstable and dominate the instability at large Mach numbers. Figure 17 shows the variation of the growth rates of secondary waves with spanwise wavenumber when the

primary wave is a first- or second-mode wave. In both cases, $F = 120 \times 10^{-6}$, $a = 0.01/\sqrt{2}$, and $\gamma_j = 0$. The first-mode primary wave and its corresponding secondary waves are calculated at $R = 1150$; the primary wave is slightly unstable. The second-mode primary wave and its corresponding secondary waves are calculated at $R = 1950$; the primary wave is very stable. It follows from Figure 17 that the maxima of the growth rates of the secondary waves are comparable. Figure 18 shows the growth rates of the free waves (secondary waves when $a = 0$). The free wave corresponding to the second-mode wave is stable for a wide range of β, whereas the free wave corresponding to the first-mode wave is slightly unstable for the same range of β. Comparing Figures 17 and 18, we conclude that a primary first-mode wave having an amplitude of $0.01/\sqrt{2}$ increases the growth rate of the secondary wave by an order of magnitude. Moreover, the presence of a primary second-mode wave strongly destabilizes the secondary wave.

When the primary wave is a first-mode wave it follows from Figure 17 that the maximum growth rate of the secondary wave occurs when $\beta = 0.199$. Figure 19 shows the variation of the secondary growth rate with frequency. The maximum growth rate increases by about 25% and shifts to an $F \approx 112 \times 10^{-6}$.

6. EFFECT OF IMPERFECTIONS ON STABILITY OF FLOWS OVER PLATES

The boundary layers over natural laminar-flow components in the presence of surface imperfections (e.g., waviness and steps) must accurately be computed so that the effect of these imperfections on the stability and transition can be evaluated. Moreover, the magnitudes of the imperfections under consideration are such that strong viscid-inviscid interaction and small separation bubbles are unavoidable. Definitely, solutions to the full Navier-Stokes equations can accurately predict such flowfields provided that the grid is so fine that important flow structures are not smeared by the truncation errors or artificial dissipation. However, the number of flow cases that needs to be investigated is very large, and this makes solving the full Navier-Stokes equations a very expensive task. A more economical alternative is to solve the interacting boundary-layer equations.

Ragab, Nayfeh and Krishna (ref. 50) investigated the accuracy of the compressible interacting boundary-layer computations and their limitations in predicting flows over surface imperfections. They compared the results of interacting boundary-layer computations with solutions to the full Navier-Stokes equations. Comparisons were made for the mean flow profiles as well as the stability characteristics such as the growth rates and amplification factors of linear stability waves.

The thin-layer compressible Navier-Stokes equations are solved using the well known computer code "ARC2D" which has been developed at NASA Ames (version 1.5 GAMMA, 72/85). The code incorporates different methods of solutions all of which are implicit in time, and it uses second-order central differences in space. Ragab et al (ref. 50) selected the method of solution in which the diagonal form of the equations are used (refs. 51,52). Mixed second- and fourth-order dissipation terms were added explicitly and implicitly, and the obtained pentadiagonal system of equations was solved directly.

Sheared Cartesian grids were used for all the cases presented here. An example is shown in Figure 20 for a smooth backward-facing step. The equation of the step is

$$y = \frac{1}{2} h(1 + \mathrm{erf} \; \bar{x}), \quad \bar{x} = \mathrm{Re}^{-3/8} \lambda^{5/4} (x - 1) \qquad (6.1)$$

658

where Re is the Reynolds number based on the distance from the leading edge to the step center (x = 1) and λ = 0.332057. The step specified by equation (6.1) is originally given by Smith and Merkin (ref. 53) who analyzed the incompressible flow using triple-deck theory. The numerical values used in Figure 20 are Re = 10^6 and h = - 0.003. We note that the y-coordinates in Figure 20 are magnified by a factor of 20 relative to the x-coordinates. The inflow boundary of the computational domain is at x $\approx$ - 0.06 (i.e., the plate leading edge x = 0 is included in the domain), and the outflow boundary is located at x = 2.0. The top boundary is placed at y $\approx$ 0.4. More details about the grid will be given in the results section.

Ragab, Nayfeh and Krishna developed a code for solving the compressible interacting boundary-layer equations. The numerical method is an extension of Veldman's method (ref. 54) to compressible flows. The salient feature of the method is the simultaneous solution of the boundary-layer equations and the inviscid flow, which is given by the small disturbance theory of compressible potential flow. A similar treatment is presented by Davis (ref. 55) and Nayfeh, Ragab, and Al-Maaitah (ref. 56).

In this subsection we compare the mean flow predicted by the Navier-Stokes code ARC2D and the interacting boundary-layer code IBL for the flow over a backward-facing step. The step is specified by equation (6.1). The step height is h = - 0.003, the Mach number is 0.5, and the Reynolds number is 10^6. The wall is assumed to be insulated.

The grid used in the IBL calculations has a uniform streamwise step size of Δx = 0.005 and a geometrically stretched grid in the η- direction, where η is the Levy-Lees variable. At the wall $\Delta\eta$ = 0.05 and the stretching factor is 1.05. Four grids are used with the Navier-Stokes solver. In grid 1 (136x70), a uniform Δx = 0.005 is used in the range 0.9 $\leq$ x $\leq$ 1.1. For x < 0.9 and x > 1.1, Δx is stretched geometrically at the rate of 1.05 provided that Δx does not exceed 0.03. If Δx exceeds 0.03, a uniform spacing Δx = 0.03 is used. The step size in the y direction is geometrically stretched between the wall and the top boundary y $\approx$ 0.4 with Δy_1 = 1.5×10^{-4}. In grid 2 (136x99), the streamwise grid is the same as in grid 1, and the y grid has 99 points between the wall and y $\approx$ 0.4 with Δy_1 = 0.3×10^{-4}. In grid 3 (166x120), the streamwise grid in the interval 0.9 $\leq$ x $\leq$ 2.0 is the same as that in grid 1 and more points are added in -.06 $\leq$ x $\leq$ 0.9 so that the number of streamwise points is 166, and the y grid has 120 points between the wall and y $\approx$ 0.4 with Δy_1 = 0.3×10^{-4}. In grid 4 (176x153), the streamwise grid is the same as that in grid 1 except Δx = 0.003, and the y grid has 153 points between the wall and y $\approx$ 0.8 with Δy_1 = 0.3×10^{-4}.

The friction-coefficient distribution on the step surface is depicted in Figure 21. We observe that there is an appreciable difference between the results predicted by ARC2D using the different grids. The trends in Figure 21 suggest that the agreement can be improved slightly if a finer grid is used with ARC2D. The results obtained using the IBL code are in good agreement with those obtained using ARC2D with the finest grid. Figure 22 compares the pressure-coefficient distribution predicted using the IBL code with that obtained using ARC2D with the finest grid. The agreement is fairly good. Thus, we conclude that the IBL code can be used to calculate accurately the mean flows over steps, humps, and troughs as long as massive separation and vortex shedding do not occur.

The stability calculations demand highly accurate velocity and temperature profiles - their magnitudes as well as their derivatives. Figure 23 compares the

spatial growth rates $-\alpha_i$ calculated at $x = 0.64$ for an $F = 80\times10^{-6}$ using the IBL predicted profiles with those calculated using the ARC2D predicted profiles with the finest grid. The agreement is very good, indicating that the IBL code predicts fairly well the magnitudes as well as the derivatives of the velocity and temperature profiles. Using these growth rates, we calculate the amplification factor N from

$$N = - \int_{R_0}^{R} 2\alpha_i \, dR$$

where $R = \sqrt{Re_x}$. The variation of the N factor calculated using the growth rates based on the profiles obtained with the IBL code is compared with those calculated using the growth rates based on the profiles obtained with the ARC2D code with the four grids in Figure 24. The latter N factor distribution seems to converge as the grid is refined to a distribution that comes closer and closer to that obtained using the growth rates based on the profiles predicted by the IBL code, providing a further credibility to the IBL procedure.

Figure 25 shows the influence of the Mach number on the N-factor distribution for the most amplified 2D wave for a backward-facing step having an $h = -0.003$ and a slope of $-4.349°$. It is clear that compressibility is stabilizing.

In Figure 26, for $M_\infty = 0.5$, we show the influence of the disturbance frequency on the N-factor distribution for waves propagating past the same backward-facing step. It is clear that the most dangerous frequency F is about 50×10^{-6}.

7. SWEPT WING BOUNDARY LAYERS

All of the numerical examples discussed in the preceding sections are concerned with the 2D and 3D stability of 2D or axisymmetric boundary-layer flows. In this section, we discuss the stability of 3D boundary layers and in particular boundary layers on transonic sweptback wings because of their aeronautical importance. The stability of 3D boundary layers differs from that of 2D boundary layers in that a 3D boundary layer is subject to crossflow instability and in that the growth direction in a 3D boundary layer need not coincide with the wave direction.

From his flight tests on aircraft with sweptback wings, Gray discovered that the boundary layer became turbulent closer to the leading edge than on a corresponding unswept wing. Using evaporation methods for indicating the state of the boundary layer, he discovered the existence of regularly spaced vortices whose axes lie in the streamwise direction. Since on a swept wing the spanwise pressure gradient deflects the boundary layer toward the region of low static pressure, the flow paths of the boundary-layer profiles differ from the potential flow streamlines and a crossflow developes in the direction normal to the streamlines (i.e., the mean flow is three-dimensional). The crossflow profiles have inflection points, making them dynamically unstable and hence leading to the generation of the vortices. This crossflow instability was confirmed in wind tunnels on large swept wings by Gregory, Stuart and Walker (ref. 34).

The feasibility of using suction to maintain laminar flow in the presence of crossflow instability was shown by Pfenninger et al (ref. 57), Bacon et al (ref. 58), Gault, and Pfenninger and Bacon (ref. 59) on a 30-deg sweptback wing. This feasibility culminated in the successful maintenance of full-chord laminar flow on an X-21 wing.

The problem of laminar-flow control on sweptback wings and the discovery of Gray of the crossflow instability stimulated research into the linear stability of three-dimensional flows. In contrast with the problem of 2-D flows, disturbances in a 3-D flow are always three-dimensional. Stuart (ref. 34) derived the general linear equations that describe the 3-D stability of 3-D incompressible boundary layers over bodies, including the effects of boundary-layer growth and body and streamline curvatures. He showed that the temporal parallel stability problem of a 3-D incompressible flow can be reduced to that of a 2-D stability problem. For a given R and ω, his transformation relates the wave numbers α and β in a 3-D flow with the streamwise and spanwise velocity components U_m and W_m to the wavenumber $k = (\alpha^2 + \beta^2)^{\frac{1}{2}}$ in a 2-D flow having the velocity $U = (\alpha U_m + \beta W_m)/k$. He used the inviscid form of these disturbance equations to explain the crossflow instability as an inflectional instability. Brown (refs. 7,16) numerically solved the temporal viscous eigenvalue problems for flows over a rotating disk and a few sweptback wing boundary layers with distributed suction.

Since the uncoupling of the crosswise stability problem from the streamwise stability problem is artificial, a number of attempts have been directed toward determining the stability of the combined streamwise and spanwise stability problems to determine the suction requirements for maintaining laminar flow over sweptback wings. The form of the 3-D disturbance is given by equations (4.3) and (4.4) leading to the dispersion relation $\omega = \omega(\alpha,\beta,x,z)$. We note that, in contrast with the case of parallel flows, α and β are functions of x and z and the phase function θ cannot be written as $\alpha x + \beta z - \omega t$. Instead α, β, and ω are related to θ as in equations (4.4).

To complete the problem formulation, one needs to specify initial conditions in addition to the governing equations and boundary conditions. For the case of a general pressure disturbance at say the curve $x = a$,

$$p(x = a, y,z,t) = P(y,z,t) \tag{7.1}$$

This arbitrary disturbance will generate a continuum of wave components of the form given by equations (4.3) and (4.4) and the observed wave motion consists of their superpositions. For the case of spatial stability in parallel mean flows, the pressure disturbance can be expressesd

$$p(x,y,z,t) = \iint \zeta_4(y;\beta,\omega)\exp[i\alpha(\beta,\omega)x + i\beta z - i\omega t]d\omega d\beta \tag{7.2}$$

On the other hand, if the initial condiitons are generated by a source (such as a vibrating ribbon) oscillating at the frequency ω (i.e., monochromatic wave) at the curve defined by $x = a$, then

$$p(x = a,y,z,t) = \tilde{P}(y,z)\exp(-i\omega t) \tag{7.3}$$

Then, for the case of parallel mean flows, the pressure disturbance can be expressed as

$$p(x,y,z,t) = \exp(-i\omega t)\iint \zeta_4(y;\beta)\exp[i\alpha(\beta)x + i\beta z]d\beta \tag{7.4}$$

661

To evaluate the integral in equation (7.2), one needs to solve the eigenvalue problem for all possible values of β and ω and then perform the integration, an expensive procedure. Similarly, to evaluate the integral in equation (7.4), one needs to solve the eigenvalue problem for all possible values of β and then perform the integration, again an expensive procedure. However, if the disturbances are sufficiently weak they will not influence transition until they have traveled a large distance from the source. Then, asymptotic methods, namely the saddle-point method, can be effectively used to determine the following approximations to the integrals in equations (7.2) and (7.4):

$$p(x,y,z,t) \propto \frac{\exp\left[i\alpha(\beta^*,\omega^*)x + i\beta^*z - i\omega^*t\right]}{x\left[\frac{\partial^2\alpha}{\partial\beta^2}\frac{\partial^2\alpha}{\partial\omega^2} - \left(\frac{\partial^2\alpha}{\partial\beta\partial\omega}\right)^2\right]^{\frac{1}{2}}} \tag{7.5}$$

where

$$\frac{z}{x} = -\frac{\partial\alpha}{\partial\beta} \quad \text{and} \quad \frac{t}{x} = \frac{\partial\alpha}{\partial\omega} \tag{7.6}$$

and

$$p(x,y,z,t) \propto \frac{\exp\left[i\alpha(\beta^*)x + i\beta^*z - i\omega t\right]}{\left[x\frac{\partial^2\alpha}{\partial\beta^2}(\beta^*)\right]^{\frac{1}{2}}} \tag{7.7}$$

where

$$\frac{z}{x} = -\frac{d\alpha}{d\beta} \tag{7.8}$$

It is clear from equations (7.6) and (7.8) that for a physical wave, $\partial\alpha/\partial\beta$ and $\partial\alpha/\partial\omega$ must be real for an arbitrary disturbance and $d\alpha/d\beta$ must be real for a monochromatic disturbance.

The preceding discussion shows that by the time the wave motion is important for transition, it has already evolved to either the state given by equation (7.5) in the case of an arbitrary disturbance (corresponding to natural transition) or the state given by equation (7.7) in the case of a monochromatic disturbance. In both cases, the disturbance is dominated by a single wave component having a fixed ω, β, and α. Using the method of multiple scales or the method of averaging to account for a weak growth of the boundary layer in x and z, one finds that by the time the wave motion is important for transition (i.e., for large x), it has evolved again to the state given by equations (4.3) and (4.4); that is, the disturbance is dominated by a wave packet centered at the frequency ω and spanwise wavenumber β. However, in this case, α, β, and A are not constants; equations (4.23), (4.29) and (4.30) describe their modulation with x, z, and t. To solve these modulation equations (Cauchy problem), one needs to specify initial conditions on non-characteristic curves.

If the initial data consist of a wavepacket centered at the frequency ω, then

$$A(x = a, z, t) = A_0(z, t), \quad \beta(x = a, z) = \beta_0(z) \tag{7.9}$$

and it follows from equations (4.23), (4.29) and (4.30) that the wave propagates along the characteristics

$$\frac{dt}{ds} = 1, \quad \frac{dx}{ds} = \omega_\alpha, \quad \frac{dz}{ds} = \omega_\beta \tag{7.10}$$

662

For a physical problem, ω_α and ω_β must be real. Along these characteristics,

$$\frac{dA}{ds} = \epsilon h_1 A, \qquad \frac{d\alpha}{ds} = \epsilon h_2, \qquad \frac{d\beta}{ds} = \epsilon h_3 \qquad (7.11)$$

If the initial data consist of a single frequency (i.e., monochromatic wave), then

$$A(x = a, z) = A_0(z), \quad \beta(x = a, z) = \beta_0(z) \qquad (7.12)$$

It follows from equations (4.29)-(4.31) that the wave propagates along the characteristics defined by equations (4.33), where $\omega_\beta/\omega_\alpha$ is real. The modulation of A, α, and β along these characteristics is governed by equations (4.32). The solution of equations (4.33) is a one-parameter family of curves.

The question arises how one can use the results of the linear stability theory for transition prediction or evaluation of proposed laminar-flow concepts and requirement on swept wings? Motivated by the success of the so-called e^N method in correlating experimental transition data in incompressible 2D flows, many investigators have attempted to extend it to 3D incompressible and compressible flows. Whereas in 2D flows, the direction of growth is known, namely, the mean flow direction, in 3D flows, the direction of growth is not known a priori. In 2D flows, one can either use spatial stability theory and calculate the spatial growth rate directly or use temporal stability theory, calculate the temporal growth rate, and then calculate the spatial growth rate using the group velocity. Integrating the spatial growth rates yields the N factors.

Srokowski and Orszag (ref. 60) developed a computer code called SALLY using the temporal incompressible stability theory. At any location on the wing, the code iterates on α and β (which are taken to be real) to yield the maximum temporal growth rate for a given dimensional frequency ω_r. Then, several frequencies are examined until a global local maximum is obtained. The resulting amplification rate is then converted into a spatial amplification rate using the real part of the group velocity, which is then integrated along a trajectory defined by the direction of the real part of the group velocity. Hefner and Bushnell (ref. 61) calibrated the results of the envelope method using available transition data on swept-back wings. Later, Malik (ref. 36) developed a code called COSAL, which is the compressible version of SALLY. Although the envelope method is easy to implement, it is artificial because one continuously hops from one wave to another. Moreover, the N factors calculated using the envelope method increase monotonically to the end of the instability region, and hence the envelope method may over estimate the amplitude ratios.

For an infinite swept wing, the mean profiles are independent of the spanwise coordinate, and hence it follows from equations (4.4) and (4.5) that β is constant. Mack (ref. 62) performed crossflow stability calculations over the forward region of a $35°$ sweptback wing using this condition and determined the N factors for a zero frquency and a band of initial wave numbers. He found that the peak value maximized over all wave numbers is 7.8 compared with 11.2, obtained using the SALLY code. In contrast with the results of the envelope method, which increase monotonically in the instability region, the results of Mack achieve a peak because he followed a given wave from a more unstable region to a less unstable region. Using the temporal theory, Lekoudis (ref. 63) and Mack (ref. 64) determined the influence of suction on

the stability of flows over sweptback wings. Lekoudis (ref. 65) ascertained the influence of cooling on the stability of flows over sweptback wings.

If the wing is not infinite, the mean flow will be a function of both spanwise and streamwise coordinates and hence α and β are functions of x and z. In this case, the wave motion will be dominated by a single frequency spatial wavepacket as discussed above. Based on this theory, Nayfeh (ref. 21) proposed a method for determining the most amplified disturbance propagating from some given initial chord location on a wing. We select one specific wave at an initial point and then follow only that one wave along its trajectory. Then, we change the initial conditions and repeat the calculations to determine the most unstable wave.

To demonstrate the method we choose β_r^*, the dimensional form of β_r, to be a constant at some initial chordwise location x = a for all z. At this initial point we still have three unspecified values β_i, α_r, and α_i. Two of these are determined through numerical integration of the disturbance equations and satisfaction of the boundary conditions through a Newton-Raphson iteration. The third is found by requiring that $\omega_\beta/\omega_\alpha$ be real. This fixes the direction of marching. From here we evaluate

$$\frac{d\alpha}{ds} = \varepsilon \frac{h_2}{\omega_\alpha} \tag{7.13}$$

$$\frac{d\beta}{ds} = \varepsilon \frac{h_3}{\omega_\alpha} \tag{7.14}$$

To stay on the initial wave, we increment the characteristic variable s by ds, evaluate dx and dz from equations (4.33), and correct α and β by

$$\alpha = \alpha + \varepsilon \frac{h_2}{\omega_\alpha} ds \tag{7.15}$$

$$\beta = \beta + \varepsilon \frac{h_3}{\omega_\alpha} ds \tag{7.16}$$

We then renondimensionalize with respect to local edge variables at the new x and z. To test that we are on the same wave, we integrate the disturbance equations at the new x and z with the new α and β to see if the boundary conditions are satisfied and $\omega_\beta/\omega_\alpha$ is real. If they are, we evaluate $d\alpha/ds$ and $d\beta/ds$, increment s, correct α and β, and continue marching along the trajectory. If these conditions are not all satisfied, we decrease the step size ds until they are and then proceed as above. Since A_0 is the amplitude of the disturbance initially, it follows from equations (4.32a) that

$$A = A_0 \exp\left(\int_a^s \varepsilon \frac{h_1}{\omega_\alpha} ds \right) \tag{7.17}$$

Hence

$$u = A_0 \zeta_1(x_1,y,z_1) \exp \left\{ \int_a^X \left[i\left(\alpha + \beta \frac{\omega_\beta}{\omega_\alpha} \right) + \varepsilon \frac{h_1}{\omega_\alpha} \right] dx - i\omega t \right\} \tag{7.18}$$

and the n-factor is given by

664

$$n = - \int_a^x [\alpha_i + \frac{\omega_\beta}{\omega_\alpha} \beta_i - \epsilon(\frac{h_1}{\omega_\alpha})_r] dx$$

As we march we compute the n-factor from where the disturbance first goes unstable

$(\frac{dn}{dx} < 0)$ to where it becomes stable again $(\frac{dn}{dx} < 0)$. Once we compute n we change β_r^*

to determine which β_r^* is associated with the largest value of n. This tells us the initial spanwise wavenumber of the most dangerous wave for a given frequency from a given chord location. Then we vary the dimensional frequency to determine the most dangerous frequency.

This approach has been implemented by Padhye and Nayfeh (ref. 66) and Reed and Nayfeh (ref. 67) for the X-21 wing with upper surface chordwise pressure coefficient and suction distribution as shown in Figures 1 and 2. A schematic of the wing is presented in Figure 3 showing the coordinate system used. This wing was designed for laminar-flow control and derived from the NACA 65A210 airfoil. The sweeps at the leading and trailing edges are 33.2 and 19.1 degrees, respectively, and the freestream velocity is 774.4 feet per second. Under the assumption of negligible spanwise (along roots) pressure gradient, there are no twist and tip and wing-body effects included in the analysis. Also they made the assumption of constant Prandtl number and specific heat at constant pressure.

Reed and Nayfeh (ref. 67) focused their attention on the aft region of the wing, specifically the 70-percent location on the 14.66-foot chord. They introduced disturbances at this point and followed them along their trajectories as described above to ascertain their stability characteristics. This initial location lies in the rear adverse chordwise pressure gradient region.

For a specific constant dimensional frequency introduced at the 70-percent chord, to find the spanwise wavenumber maximizing the amplification factor, they consider the wavenumber resulting in local maximum temporal growth rate. That is, they took the frequency ω to be complex and the two wave numbers α and β to be real. They specified ω_r and iterated on α, β and ω_i to satisfy the boundary conditions and the condition that $\omega_\beta/\omega_\alpha$ be real. Then they converted to spatial stability and marched along the direction defined by the group velocity, which is kept real as described above. The amplification factor was computed in marching. This process was done for a whole gamut of frequencies until the frequency with maximum amplification factor was identified. Figure 4 shows results of frequency plotted versus spanwise wavenumber causing maximum growth for disturbances introduced at the 70-percent-chord location. The distribution appears to be linear.

As a result of searching, they found that the most unstable disturbance introduced at 70-percent chord is the one with a frequency of about 330 hertz and spanwise wavenumber of 272 per foot. Figure 5 shows disturbance amplification ratios for frequencies in this neighborhood. If the stability was performed using incompressible theory, the most unstable frequency would be about 200 Hz. The addition of compressibility increases the frequency of the most unstable disturbance. Moreover, compressibility significantly reduces the growth rates and amplification factors.

ACKNOWLEDGEMENT

666

$$a_{12} = a_{56} = a_{78} = 1$$

$$a_{21} = \alpha^2 + \beta^2 - i\hat{\omega}R/\mu_m T_m$$

$$a_{22} = - Du_m/\mu_m$$

$$a_{23} = - i\alpha(m + 1)DT_m/T_m - i\alpha D\mu_m/\mu_m + RDU_m/\mu_m T_m$$

$$a_{24} = i\alpha R/\mu_m + (m + 1)\gamma M_\infty^2 \alpha\hat{\omega}$$

$$a_{25} = - \alpha(m + 1)\hat{\omega}/T_m - D(\mu_m' DU_m)/\mu_m$$

$$a_{26} = - \mu_m' DU_m/\mu_m$$

$$a_{31} = - i\alpha$$

$$a_{33} = DT_m/T_m$$

$$a_{34} = i\gamma M_\infty^2 \hat{\omega}$$

$$a_{35} = - i\hat{\omega}/T_m$$

$$a_{37} = - i\beta$$

$$a_{41} = - i\chi\alpha(rDT_m/T_m + 2D\mu_m/\mu_m)$$

$$a_{42} = - i\chi\alpha$$

$$a_{43} = \chi\left[- \alpha^2 - \beta^2 + i\hat{\omega}R/\mu_m T_m + rD^2 T_m/T_m + rD\mu_m DT_m/\mu_m T_m\right]$$

$$a_{44} = - i\chi r\gamma M_\infty^2\left[\alpha DU_m + \beta DW_m - \hat{\omega}DT_m/T_m - \hat{\omega}D\mu_m/\mu_m\right]$$

$$a_{45} = i\chi\left[r(\alpha DU_m + \beta DW_m)/T_m + \mu_m'(\alpha DU_m + \beta DW_m)/\mu_m - r\hat{\omega}D\mu_m/\mu_m T_m\right]$$

$$a_{46} = - i\chi r\hat{\omega}/T_m$$

$$a_{47} = - i_\chi r\beta DT_m/T_m - 2i_\chi \beta D\mu_m/\mu_m$$

$$a_{48} = - i_\chi \beta$$

$$a_{62} = - 2(\gamma - 1)M_\infty^2 Pr DU_m$$

$$a_{63} = - 2i(\gamma - 1)M_\infty^2 Pr(\alpha DU_m + \beta DW_m) + RPr\ DT_m/\mu_m T_m$$

$$a_{64} = i(\gamma - 1)M_\infty^2 Pr R\hat{\omega}/\mu_m$$

$$a_{65} = \alpha^2 + \beta^2 - iRPr\hat{\omega}/\mu_m T_m - (\gamma - 1)M_\infty^2 Pr\mu_m'[(DU_m)^2 + (DW_m)^2]/\mu_m$$

$$- D^2\mu_m/\mu_m$$

$$a_{66} = - 2D\mu_m/\mu_m$$

$$a_{68} = - 2(\gamma - 1)M_\infty^2 Pr DW_m$$

$$a_{83} = - i(m + 1)\beta DT_m/T_m - i\beta D\mu_m/\mu_m + RDW_m/\mu_m T_m$$

$$a_{84} = (m + 1)\gamma M_\infty^2 \beta\hat{\omega} + i\beta R/\mu_m$$

$$a_{85} = - (m + 1)\beta\hat{\omega}/T_m - D(\mu_m'DW_m)/\mu_m$$

$$a_{86} = - \mu_m'DW_m/\mu_m$$

$$a_{87} = \alpha^2 + \beta^2 - i\hat{\omega}R/\mu_m T_m$$

$$a_{88} = - D\mu_m/\mu_m$$

where
$$\mu_m' = d\mu_m/dT_m, \quad DF = \partial F/\partial y,$$

and
$$\hat{\omega} = \omega - \alpha U_m - \beta W_m, \quad \chi = [R/\mu_m - ir\gamma M_\infty^2 \hat{\omega}]^{-1}$$

$$D_n = i \sum_{m=1}^{8} \frac{\partial a_{nm}}{\partial \omega} \zeta_m$$

$$E_n = -i \sum_{m=1}^{8} \frac{\partial a_{nm}}{\partial \alpha} \zeta_m$$

$$F_n = -i \sum_{m=1}^{8} \frac{\partial a_{nm}}{\partial \beta} \zeta_m$$

where small terms $O(R^{-1})$ can be neglected. The a_{nm} are given in Appendix A.

$$G_1 = G_5 = G_7 = 0$$

$$G_2 = \frac{R}{\mu_m} \left[\frac{U_m}{T_m} \frac{\partial \zeta_1}{\partial x_1} + \frac{\zeta_1}{T_m} \frac{\partial U_m}{\partial x_1} + \frac{V_m}{T_m} \frac{\partial \zeta_1}{\partial y} + \frac{\zeta_7}{T_m} \frac{\partial U_m}{\partial z_1} \right.$$

$$+ \frac{W_m}{T_m} \frac{\partial \zeta_1}{\partial z_1} + \frac{\partial \zeta_4}{\partial x_1} + \left(\frac{\gamma M_e^2 \zeta_4}{T_m} - \frac{\zeta_5}{T_m^2} \right) \left(U_m \frac{\partial U_m}{\partial x_1} + V_m \frac{\partial U_m}{\partial y} \right.$$

$$\left. \left. + W_m \frac{\partial U_m}{\partial z_1} \right) \right] + O(1)$$

$$G_3 = \frac{\zeta_1}{T_m} \frac{\partial T_m}{\partial x_1} - \frac{\partial \zeta_1}{\partial x_1} - U_m \gamma M_e^2 \left(\frac{\partial \zeta_4}{\partial x_1} - \frac{\zeta_4}{T_m} \frac{\partial T_m}{\partial x_1} \right) + \frac{U_m}{T_m} \frac{\partial \zeta_5}{\partial x_1}$$

$$- \frac{2U_m \zeta_5}{T_m^2} \frac{\partial T_m}{\partial x_1} - \left(\frac{\partial U_m}{\partial x_1} + \frac{\partial V_m}{\partial y} + \frac{\partial W_m}{\partial z_1} \right) \left(\gamma M_e^2 \zeta_4 - \frac{\zeta_5}{T_m} \right)$$

$$- V_m \left(\gamma M_e^2 \frac{\partial \zeta_4}{\partial y} - \frac{\gamma M_e^2 \zeta_4}{T_m} \frac{\partial T_m}{\partial y} - \frac{1}{T_m} \frac{\partial \zeta_5}{\partial y} + \frac{\partial \zeta_5}{T_m^2} \frac{\partial T_m}{\partial y} \right)$$

$$- \gamma M_e^2 W_m \left(\frac{\partial \zeta_4}{\partial z_1} - \frac{\zeta_4}{T_m} \frac{\partial T_m}{\partial z_1} \right) + \frac{\zeta_7}{T_m} \frac{\partial T_m}{\partial z_1} + \frac{W_m}{T_m} \frac{\partial \zeta_5}{\partial z_1}$$

$$- \frac{2W_m \zeta_5}{T_m^2} \frac{\partial T_m}{\partial z_1} - \frac{\partial \zeta_7}{\partial z_1} + U_m \frac{\zeta_5}{T_m} \gamma M_e^2 \left(\frac{\partial P_m}{\partial x_1} + \frac{\partial P_m}{\partial z_1} \right)$$

$$- \gamma M_e^2 \left(\zeta_1 \frac{\partial P_m}{\partial x_1} + \zeta_7 \frac{\partial P_m}{\partial z_1} \right) + O(R^{-1})$$

$$G_4 = - \frac{1}{T_m} \left[U_m \frac{\partial \zeta_3}{\partial x_1} + V_m \frac{\partial \zeta_3}{\partial y} + \zeta_3 \frac{\partial V_m}{\partial y} + W_m \frac{\partial \zeta_3}{\partial z} \right] + O(R^{-1})$$

$$G_6 = - \frac{RPr}{\mu_m} \left[- \frac{\zeta_1}{T_m} \frac{\partial T_m}{\partial x_1} - \frac{U_m}{T_m} \frac{\partial \zeta_5}{\partial x_1} - \frac{V_m}{T_m} \frac{\partial \zeta_5}{\partial y} - \frac{\zeta_7}{T_m} \frac{\partial T_m}{\partial z_1} \right.$$

$$- \frac{W_m}{T_m} \frac{\partial \zeta_5}{\partial z_1} - \left(\frac{\gamma M_e^2 \zeta_4}{T_m} - \frac{\zeta_5}{T_m^2} \right) \left(U_m \frac{\partial T_m}{\partial x_1} + V_m \frac{\partial T_m}{\partial y} \right.$$

$$\left. + W_m \frac{\partial T_m}{\partial z_1} \right) + (\gamma - 1) M_e^2 \left(\frac{\partial P_m}{\partial x_1} \zeta_1 + U_m \frac{\partial \zeta_4}{\partial x_1} \right.$$

$$\left. \left. + V_m \frac{\partial \zeta_4}{\partial y} + \frac{\partial P_m}{\partial z_1} \zeta_7 + W_m \frac{\partial \zeta_4}{\partial z_1} \right) \right] + O(1)$$

$$G_8 = \frac{R}{\mu_m} \left[\frac{U_m}{T_m} \frac{\partial \zeta_7}{\partial x_1} + \frac{\zeta_1}{T_m} \frac{\partial W_m}{\partial x_1} + \frac{V_m}{T_m} \frac{\partial \zeta_7}{\partial y} + \frac{W_m}{T_m} \frac{\partial \zeta_7}{\partial z_1} \right.$$

$$+ \frac{\zeta_7}{T_m} \frac{\partial W_m}{\partial z_1} + \frac{\partial \zeta_4}{\partial z_1} + \left(\frac{\gamma M_e^2 \zeta_4}{T_m} - \frac{\zeta_5}{T^2} \right) \left(U_m \frac{\partial W_m}{\partial x_1} + V_m \frac{\partial w_m}{\partial y} \right.$$

$$\left. \left. + W_m \frac{\partial W_m}{\partial z_1} \right) \right] + O(1)$$

$$g_1 = i \sum_{m,n=1}^{8} \int_0^\infty \frac{\partial a_{nm}}{\partial \omega} \zeta_m \zeta_n^* dy$$

$$g_2 = - i \sum_{m,n=1}^{8} \frac{\partial a_{nm}}{\partial \alpha} \zeta_m \zeta_n^* dy$$

$$g_3 = - i \sum_{m,n=1}^{8} \int_0^\infty \frac{\partial a_{nm}}{\partial \beta} \zeta_m \zeta_n^* dy$$

$$\omega_\alpha = g_2/g_1, \quad \omega_\beta = g_3/g_1$$

$$h_1 = - g_1^{-1} \sum_{m=1}^{8} \int_0^\infty G_m \zeta_m^* dy$$

$$h_2 = i g_1^{-1} \sum_{m,n=1}^{8} \int_0^\infty \frac{\partial a_{nm}}{\partial x_1} \bigg|_{\alpha,\beta} \zeta_m \zeta_n^* dy$$

$$h_3 = i g_1^{-1} \sum_{m,n=1}^{8} \int_0^\infty \frac{\partial a_{nm}}{\partial z_1} \bigg|_{\alpha,\beta} \zeta_m \zeta_n^* dy$$

The a_{nm} are defined in Appendix A. The G_m are defined in Appendix B.

REFERENCES

1. Küchemann, D.: Störungsbewegungen in einer Gasströmung mit Grenzschicht, ZAMM, Vol. 18, 1938, pp. 207-222.

2. Lees, L. and Lin, C. C.: Investigation of the Stability of the Laminar Boundary Layer in a Compressible Fluid. NACA Technical Note, No. 1115, 1946.

3. Lees, L.: The Stability of the Laminar Boundary Layer in a Compressible Fluid. NACA Technical Report 876 and NACA TN1360, 1947.

4. Dunn, D. W. and Lin, C. C.: On the Stability of the Laminar Boundary Layer in a Compressible Fluid. Journal of Aeronautical Sciences, Vol. 22, 1955, p. 455.

5. Reshotko, E.: Stability of the Compressible Laminar Boundary Layer. California Institute of Technology, Guggenheim Aeronautical Laboratory, GALCIT Memorandum, 1960, p. 52.

6. Lees, L. and Reshotko, E.: Stability of the Compressible Laminar Boundary Layer. Journal of Fluid Mechanics, Vol. 12, 1962, p. 555.

7. Brown, W. B.: A Stability Criterion for Three-Dimensional Laminar Boundary Layers. Boundary Layer and Flow Control, Vol. 2, G. V. Lachmann ed. (Pergamon Press, New York) 1961, p. 913.

8. Mack, L. M: Numerical Calculation of the Stability of the Compressible Laminar Boundary Layer. California Institute of Technology, Jet Propulsion Laboratory, Report 20-122, 1960.

9. Mack, L. M.: Computation of the Stability of the Laminar Compressible Boundary Layer. Methods in Computational Physics, Vol. 4, Academic Press, 1965, p. 247.

10. Mack, L. M.: The Stability of the Compressible Boundary Layer According to a Direct Numerical Solution. AGARDograph, Vol. 97, Part 1, 1965, p. 483.

11. Mack, L. M.: Boundary-Layer Stability Theory. Jet Propulsion Lab. Document 900-277 (Rev. A), Pasadena, CA, 1969.

12. Mack, L. M.: Linear Stability Theory and the Problem of Supersonic Boundary-Layer Transition. AIAA Journal, Vol. 13, 1975, p. 278.

13. Mack, L. M.: Numerical Solution of Compressible Boundary-Layer Stability. Proceedings of Boundary-Layer Transition Group Meeting, W. D. McCauley ed., Air Force Report BSD-TR-67-213, 1967.

14. Mack, L. M.: Review of Linear Compressible Stability Theory. In Stability of Time Dependent and Spatially Varying Flows (D. L. Dwoyer and M. Y. Hussaini, eds.), Springer-Verlag, New York, 1985, pp. 164-187.

15. Mack, L. M: Boundary-Layer Linear Stability Theory. In Special Course on Stability and Transition of Laminar Flow, AGARD Report No. 709, 1984, pp. 3-1 to 3-81.

16. Brown, W. B.: Stability of Compressible Boundary Layers. AIAA Journal, Vol. 5, 1967, p. 1753.

17. Gunness, R. C.: The Stability Equations for High Mach Number Boundary-Layer Flow. Boeing Document D6-20652, Boeing Corporation, Seattle, WA, 1968.

18. Boehman, L. I.: Recalcuation of Brown's Stability Results. Proceedings of the 12th Midwest Mechanical Conference, University of Notre Dame Press, Notre Dame, IN, Vol. 6, 1971, p. 193.

19. El-Hady, N. M. and Nayfeh, A. H.: Nonparallel Stability of Compressible Boundary Layer Flows. AIAA Paper No. 80-0277, 1980.

20. Gaponov, S. A.: The Influence of Flow Non-Parallelism on Disturbance Development in the Supersonic Boundary Layer. Proceedings of the Eighth Canadian Congress of Applied Mechanics, 1981, pp. 673-674.

21. Nayfeh, A. H.: Stability of Three-Dimensional Boundary Layers. AIAA Journal, Vol. 18, 1980, pp. 406-416.

22. El-Hady, N. M.: On the Stability of Three-Dimensional, Compressible Nonparallel Boundary Layers. AIAA Paper No. 1374, 1980.

23. Laufer, J. and Vrebalovich, T.: Stability and Transition of a Supersonic Laminar Boundary Layer on an Insulated Flat Plate. Journal of Fluid Mechanics, Vol. 9, 1960, p. 257.

24. Kendall, J. M.: Wind Tunnel Experiments Relating to Supersonic and Hypersonic Boundary-Layer Transition. AIAA Journal, Vol. 13, 1975, p. 290.

25. Kendall, J. M.: Supersonic Boundary-Layer Stability Experiments. Proceedings of Boundary Layer Transition Study Group Meeting, ed. W. D. McCauley, Air Force Report BSD-TE-67-213, Aerospace Report TR 0158 (S3816-63)-1 II, 1967.

26. Demetriades, A.: An Experiment on the Stability of Hypersonic Laminar Boundary Layers. Journal of Fluid Mechanics, Vol. 7, 1960, p. 385.

27. Demetriades, A.: Hypersonic Viscous Flow Over a Slender Cone, Part III: Laminar Instability and Transition. AIAA Paper No. 74-535, 1974.

28. Demetriades, A.: Laminar Boundary Layer Stability Measurements at Mach 7 Including Wall Temperature Effects. AFOSR-TR-77-1311, 1977.

29. Lebiga, V. A., Maslov, A. A., and Pridanov, V. G.: Experimental Study of Stability of Supersonic Boundary Layers on a Plate with Blunted Leading Edge. (In Russian), Meck. Zhid i Gaza, Vol. 4, 1977, p. 65.

30. Stetson, K. F., Thompson, E. R., Donaldson, J. C., and Siler, L. G.: Laminar Boundary Layer Stability Experiments on a Cone at Mach 8. Part 1. Sharp Cone. AIAA Paper 83-1761, 1983.

31. Stetson, K. F., Thompson, E. R., Donaldson,J. C., and Siler, L. G.: Laminar Boundary Layer Stability Experiments on a Cone at Mach 8. Part 2. Blunt Cone. AIAA Paper 84-0006, 1984.

32. Stetson, K. F., Thompson, E. R., Donaldson, J. C., and Siler, L. G.: Laminar Boundary Layer Stability Experiments on a Cone at Mach 8. Part 3. Sharp Cone at Angle of Attack. AIAA Paper 85-0492, 1985.

33. Stetson, K. F., Thompson, E. R., Donaldson, J. C., and Siler, L. G.: Laminar Boundary Layer Stability Experiments on a Cone at Mach 8. Part 4. On Unit Reynolds Number and Environmental Effects. AIAA Paper 86-1087, 1986.

34. Gregory, N., Stuart, J. T., and Walker, W. S.: On the Stability of Three-Dimensional Boundary Layers with Application to the Flow Due to a Rotating Disk. Proc. Roy. Soc. London, Vol. A28, 1955, pp. 155.

35. Malik, M. R. and Orszag, S. A.: Efficient Computation of the Stability of Three-Dimensional Compressible Boundary Layers. AIAA Paper No. 81-1277, 1981.

36. Malik, M. R.: COSAL - A Black-Box Compressible Stability Analysis Code for Transition Prediction in Three-Dimensional Boundary Layers. NASA CR-165925, 1982.

37. Nayfeh, A. H.: Perturbation Methods, Wiley-Interscience, New York, 1973.

38. Nayfeh, A. H., Introduction to Perturbation Techniques, Wiley-Interscience, New York (1981).

39. Nayfeh, A. H.: Three Dimensional Stability of Growing Boundary Layers. Laminar-Turbulent Transition, R. Eppler and H. Fasel, Eds. (Springer-Verlag, New York) 1980, p. 201.

40. Nayfeh, A. H. and Padhye, A. R.: The Relation Between Temporal and Spatial Stability in Three-Dimensional Flows. AIAA Journal, Vol. 17, 1979, pp. 1084-1090.

41. Wazzan, A. R., Taghavi, H., and Keltner, G.: The Effect of Mach Number on the Spatial Stability of Adiabatic Flat Plate Flow to Oblique Disturbances. Physics of Fluids, Vol. 27, 1984, pp. 331-341.

42. Mack, L. M.: Remarks on Disputed Numerical Results in Compressible Boundary-Layer Stability Theory. Physics of Fluids, Vol. 27, 1984, pp. 342-347.

43. Malik, M. R.: Prediction and Control of Transition in Hypersonic Boundary Layers. AIAA Paper 87-1414, 1987.

44. Cebeci, T. and Stewartson, K.: On Stability and Transition in Three-Dimensional Flows. AIAA Journal, Vol. 18, 1980, pp. 398-405.

45. Nayfeh, A. H. and Harper, R.: Secondary Instability of Compressible Boundary Layers. Accepted for publication, Physics of Fluids, 1989.

46. Herbert, Th.: Subharmonic Three-Dimensional Disturbances in Unstable Plane Sheaer Flows. AIAA Paper No. 83-1759, 1983.

47. Herbert, T.: Analysis of the Subharmonic Route to Transition in Boundary Layers. AIAA Paper No. 84-0009, 1984.

48. Nayfeh, A. H. and Masad, J.:   Subharmonic Instability in Boundary Layers. Accepted for publication, Physics of Fluids, 1989.

49. Kachanov, Yu. S. and Levchenko, V. Ya.: The Resonant Interaction of Disturbances at Laminar-Turbulent Transition in a Boundary Layer. Journal of Fluid Mechanics, Vol. 138, 1984, p. 200.

50. Ragab, S. A., Nayfeh, A. H., and Krishna, R.: Influence of Smooth Steps on the Stability of Compressible Boundary Layers. Accepted for publication, Physics of Fluids, 1989.

51. Pulliam, T. H.:   Euler and Thin Layer Navier-Stokes Codes: ARC2D, ARC3D. Notes for Compl. Fluid Dyn. User's Workshop, The Univ. of Tn Space Inst., TN, 1984.

52. Pulliam, T. H. and Chaussee, D. S.:   A Diagonal Form of Implicit Approximate Factorization Algorithm. Journal of Computational Physics, Vol. 39, 1981, p. 347.

53. Smith, F. T. and Merkin, J. H.:   Triple-Deck Solutions for Subsonic Flow Past Humps, Steps, Concave or Convex Corners and Wedged Trailing Edges. Journal of Computational Physics, Vol. 10, 1982, p. 7-25.

54. Veldman, A. E. P.:   A Numerical Method for the Calculation of Laminar, Incompressible Boundary Layers with Strong Viscous-Inviscid Interaction. Report NLR TR 79023, National Aerospace Lab., The Netherlands, 1979.

55. Davis, R. T.:   A Procedure for Solving the Compressible Interacting Boundary-Layer Equations for Subsonic and Supersonic Flows. AIAA Paper No. 84-1614, 1984.

56. Nayfeh, A. H., Ragab, S. A., and Al-Maaitah, A.:   Effect of Bulges on the Stability of Boundary Layers. Physics of Fluids, Vol. 31, No. 4, 1988, pp. 796-806.

57. Pfenninger, W., Gross, L., and Bacon, T. W.:   Experiments on a 30° Swept 12 Percent Thick Symmetrical Laminar Suction Wing in the 5-ft. by 7-ft. Michigan Tunnel. Northrop Corporation, Norvair Division Report NAI-57-317 (BLC-93), 1957.

58. Bacon, J. W., Tucker, V. L., and Pfenninger, W.:   Experiments on a 30° Sept 12 Percent Thick Symmetrical Laminar Suction Wing in the 5-ft. by 7-ft. University of Michigan Tunnel.   Northrop Corporation, Norvair Division Report NOR-59-328 (BLC-119), 1959.

59. Gault, D. E.:   An Experimental Investigation of Boundary Layer Control for Drag Reduction of a Swept Wing Section at Low Speed and High Reynolds numbers. NASA TN D-320, 1960.

60. Srokowski, A. J. and Orszag, A. A.:   Mass Flow Requirements for LFC Wing Design. AIAA Paper No. 77-1222, 1977.

61. Hefner, J. N. and Bushnell, D. M.:   Application of Stability Theory to Laminar Flow Control. AIAA Paper No. 79-1493, 1979.

62. Mack, L. M.:   On the Stability of the Boundary Layer on a Transonic Swept Wing. AIAA Paper No. 79-0264, 1979.

63. Lekoudis, S. G.:   Stability of Three-Dimensional Compressible Boundary Layers over Wings with Suction.   AIAA Paper No. 79-0265, 1979.

64. Mack, L. M.:   Compressible Boundary-Layer Stability Calculations for Sweptback Wings with Suction.   AIAA Paper No. 81-0196, 1981.

65. Lekoudis, S.G.: Stability of the Boundary Layer on a Swept Wing with Wall Cooling.   AIAA Journal, Vol. 18, 1980, pp. 1029-1035.

66. Padhye, A. R. and Nayfeh, A. H.:   Nonparallel Stability of Three-Dimensional Flows.   AIAA Paper No. 81-1281, 1981.

67. Reed, H. L. and Nayfeh, A. H.:   Stability of Compressible Three-Dimensional Boundary-Layer Flows.   AIAA Paper No. 82-1009, 1982.
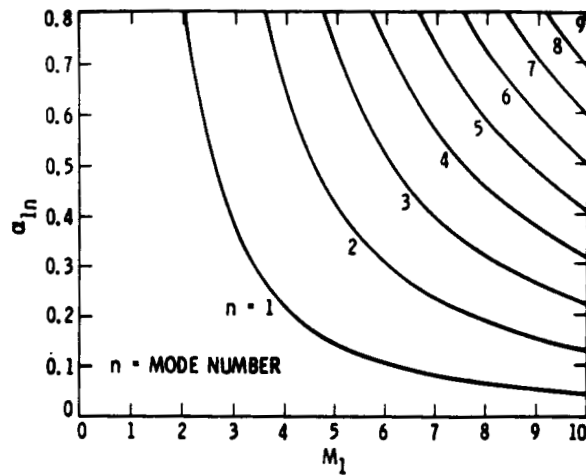
Figure 1. Multiple wave numbers of 2D noninflectional neutral waves (c=1). Insulated wall, wind tunnel temperatures, calculations of Mack (ref. 11).
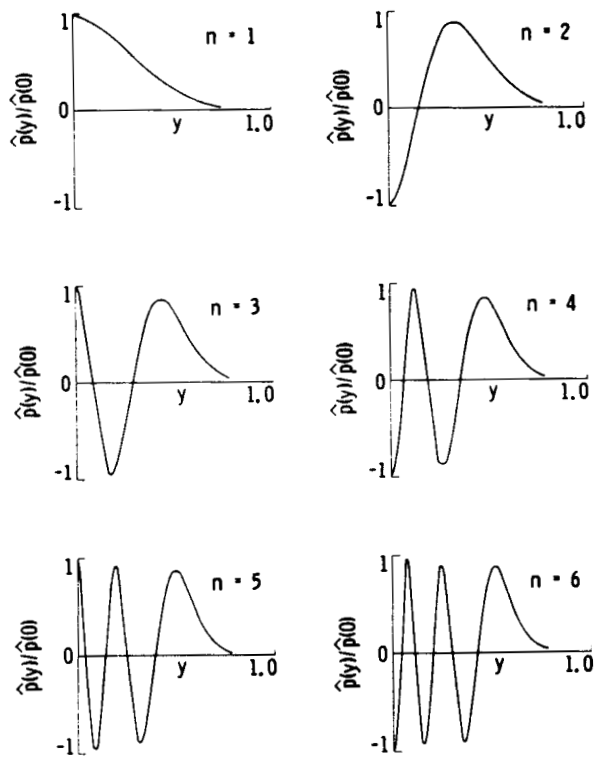
Figure 2. Pressure-fluctuation eigenfunctions of first six modes of 2D noninflectional neutral waves (c=1) at M_∞ = 10. Insulated wall, T_∞^* = 50°K, calculations of Mack (ref. 11).
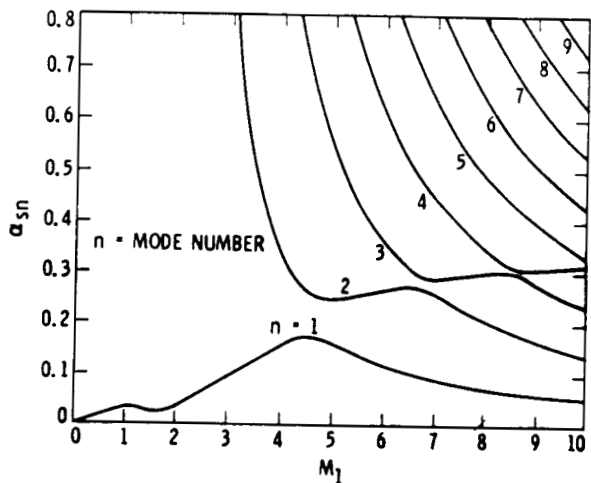
Figure 3. Multiple wave numbers of 2D inflectional neutral waves $(c=c_s)$. Insulated wall, wind tunnel temperatures, calculations of Mack (ref. 11).
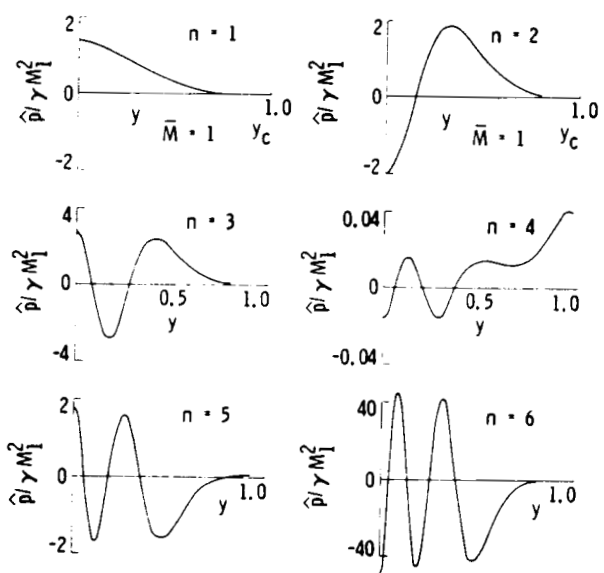
Figure 4. Pressure-fluctuation eigenfunctions of first six modes of 2D inflectional neutral waves $(c=c_s)$ at $M_\infty = 10$. Insulated wall, $T_\infty^* = 50°K$, calculations of Mack (ref. 11).
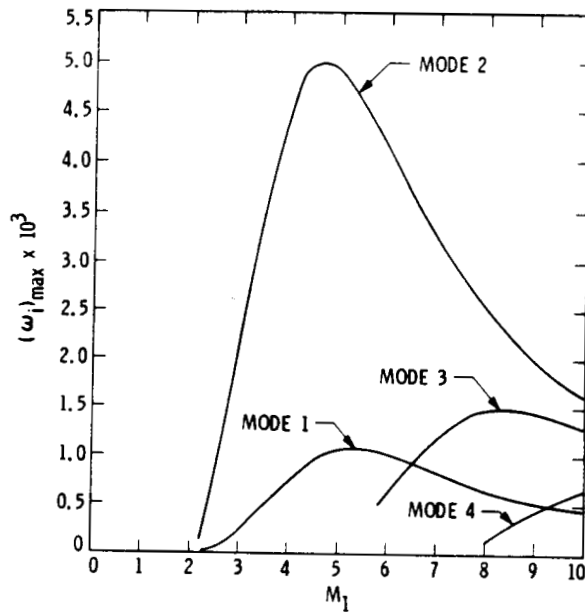
Figure 5.   Effect of Mach number on maximum temporal amplification rate of 2D waves
for first four modes.   Insulated wall, wind tunnel temperatures (ref.
11).
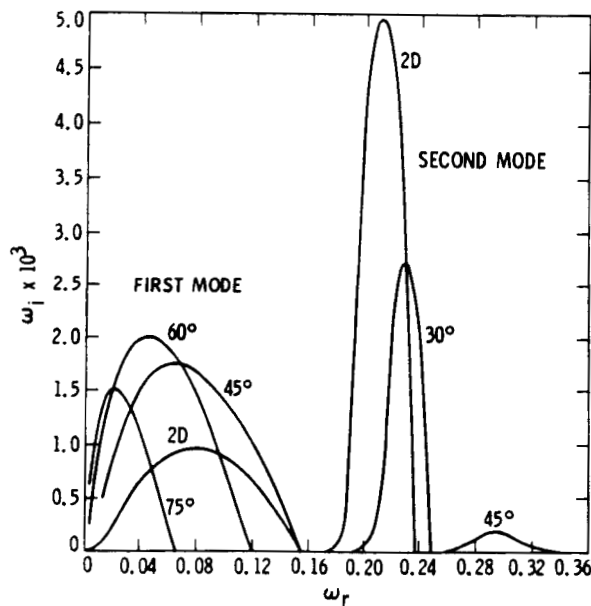
Figure 6.   Temporal amplification rate of first and second modes versus frequency
for several wave angles at M_∞ = 4.5.   Insulated wall, T_∞^* = 311°K (ref.
11).
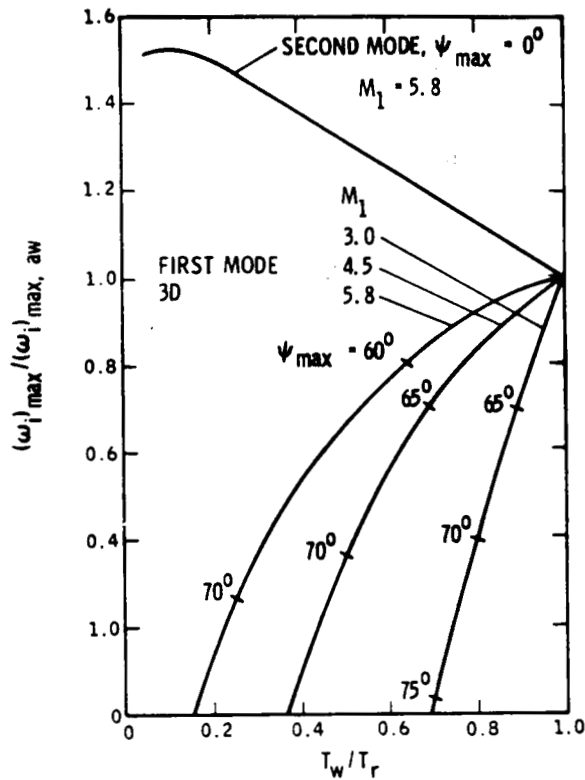
Figure 7. Effect of wall cooling on ratio of maximum temporal amplification rate with respect to both frequency and wave angle of first and second modes at M_∞ = 3.0, 4.5 and 4.8 to insulated-wall maximum amplification rate. Wind tunnel temperatures (ref. 11).
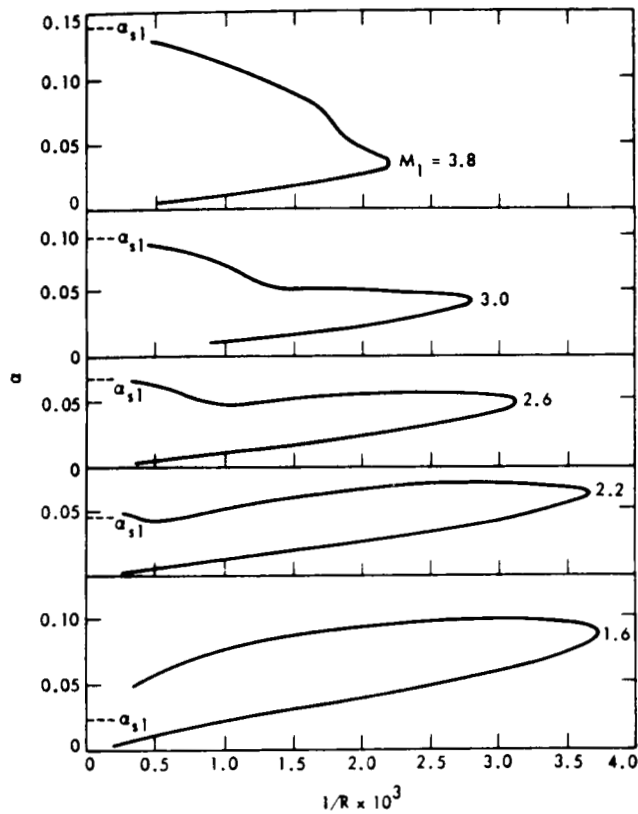
Figure 8. Two-dimensional neutral-stability curves at M_∞ = 1.6, 2.2, 2.6, 3.0, and 3.8; α_{s1} is the first neutral inviscid wavenumber with $c = c_s$ (ref. 11).
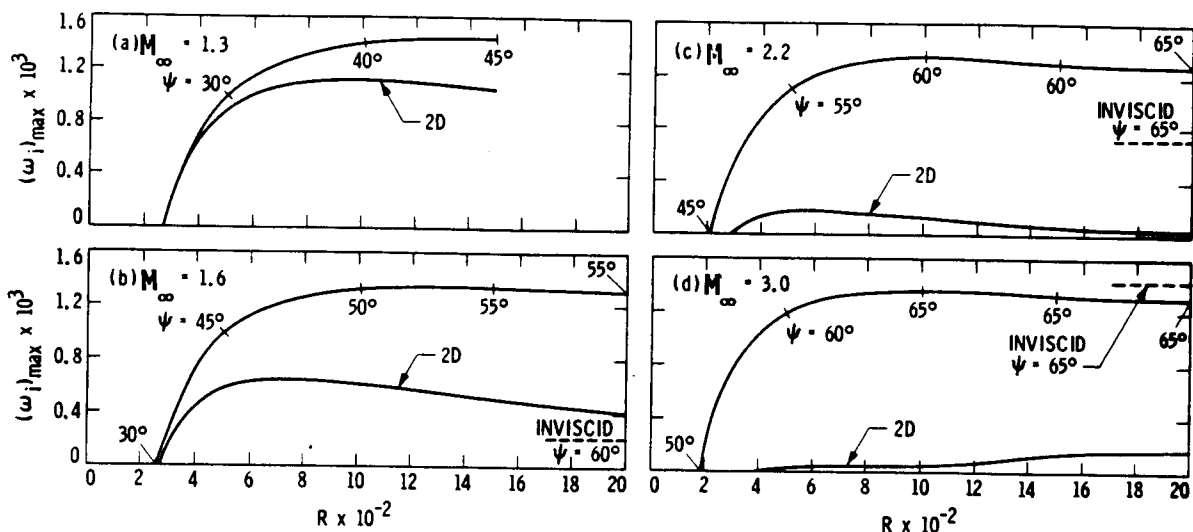
Figure 9. Distribution of maximum temporal amplification rate with Reynolds number at (a) M_∞ = 1.3, (b) M_∞ = 1.6, (c) M_∞ = 2.2 and (d) M_∞ = 3.0 for 2D and 3D waves. Insulated wall, wind tunnel temperatures (ref. 15).
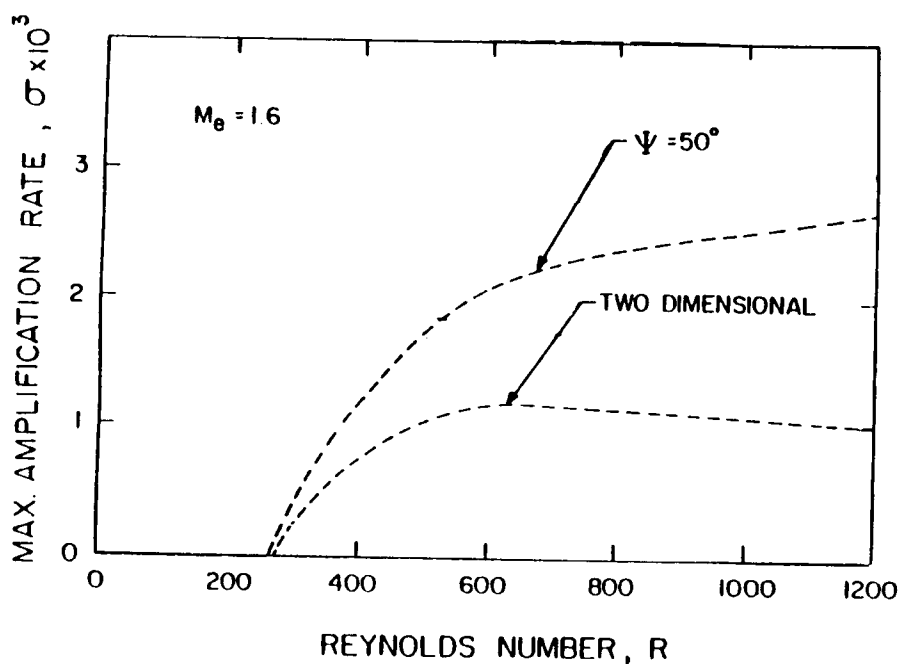
Figure 10. Variation of the maximum spatial amplification rate (with respect to frequency) with streamwise position at M_∞ = 1.6 for an oblique wave at ψ = 50° and a two-dimensional wave (ref. 19)

681
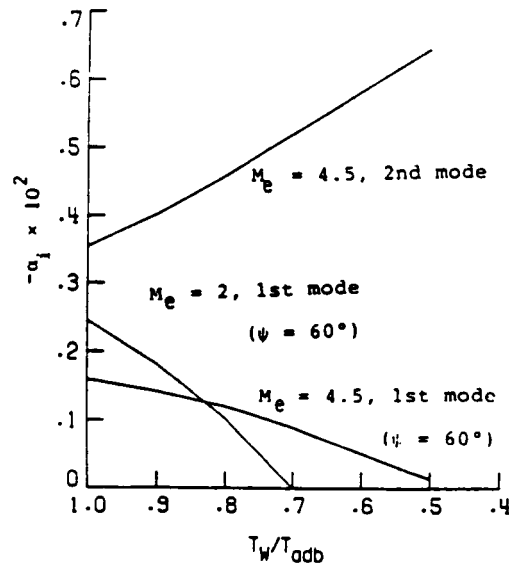
Figure 11. Effect of wall cooling on the most amplified first and second mode disturbances in a flat plate boundary layer at R = 1500 (ref. 43).
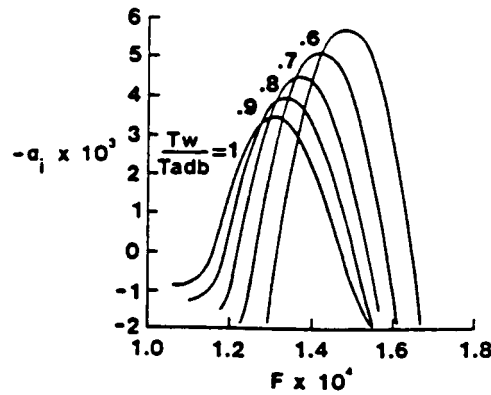
Figure 12. Effect of wall cooling on second mode instability in a boundary layer at M_e = 4.5 and R = 1500 (ref. 43).
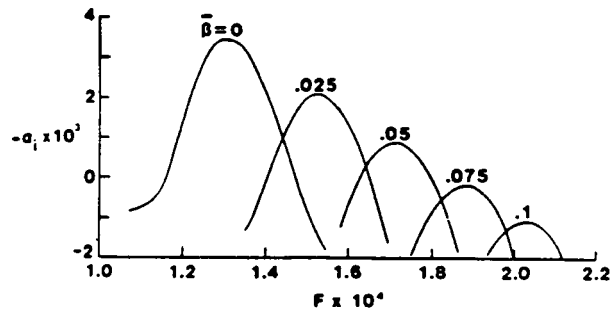
Figure 13. Effect of pressure gradient on the second mode instability in a boundary layer at M_e = 4.5 and R = 1500 (ref. 43).

682
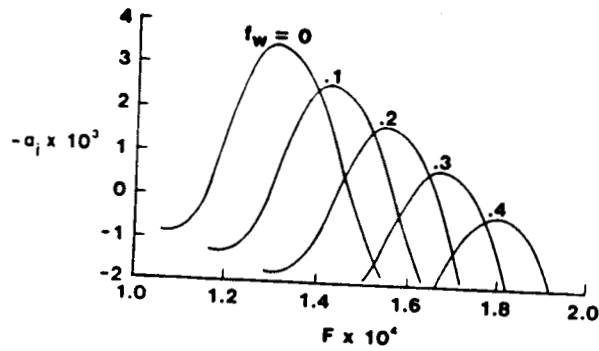
Figure 14.   Effect of wall suction on the second mode instability in a boundary layer at M_e = 4.5 and R = 1500 (ref. 43).
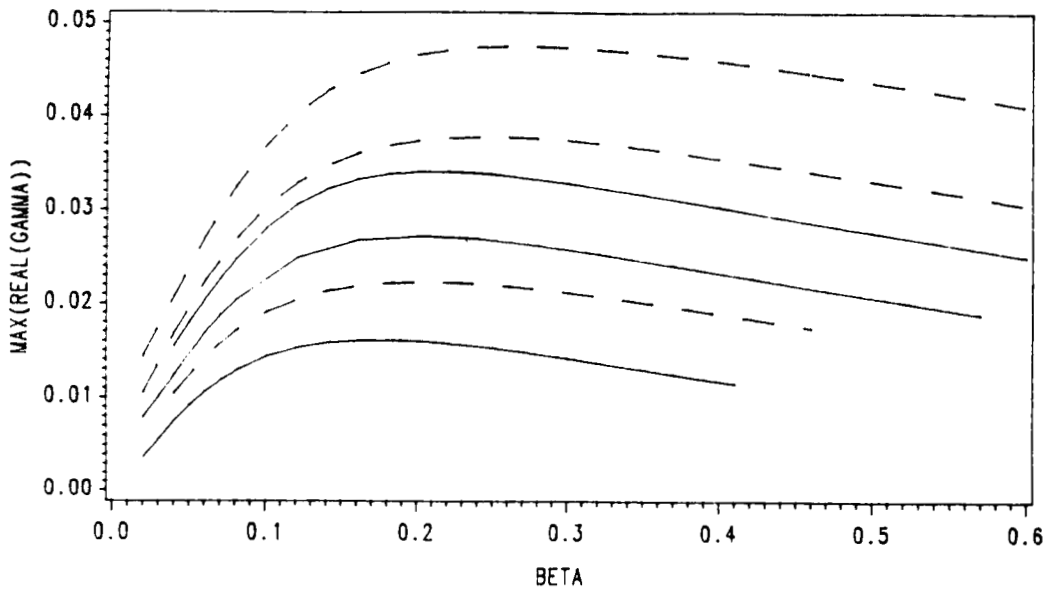
Figure 15.   Variation of the maximum growth rate of secondary waves with spanwise wavenumber for three Mach numbers and two amplitudes a of the primary wave at R = 1048.8 and an F = 83x10^{-6} for the primary wave.   Dashed curves - a = 0.02/$\sqrt{2}$ and solid curves - a = 0.01/$\sqrt{2}$.   Mach numbers for each set proceeding downward are M_∞ = 0, 0.8, and 1.6.
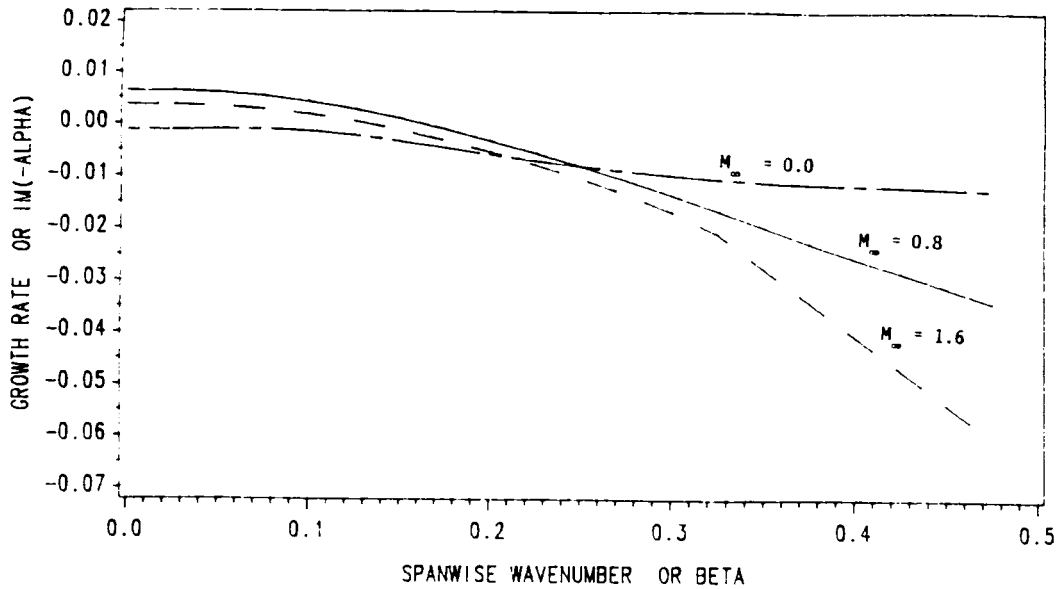
Figure 16. Variation of the growth rate of the free wave with spanwise wavenumber at R = 1048.8 and an F = 42.5x10^{-5} for three Mach numbers.
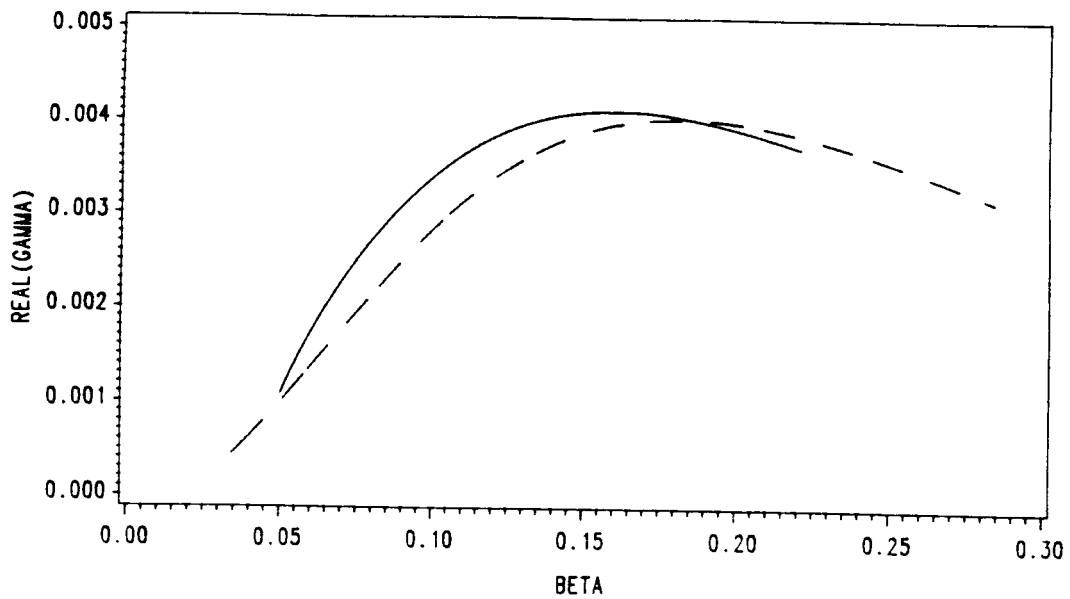
Figure 17. Variation of the growth rate of secondary waves with spanwise wave number for M_∞ = 4.5; the amplitude and frequency of the primary wave are a = 0.01/√2 and F = 120x10^{-5}: (a) first-mode primary wave at R = 1150 and (b) second-mode primary wave at 1950.

684
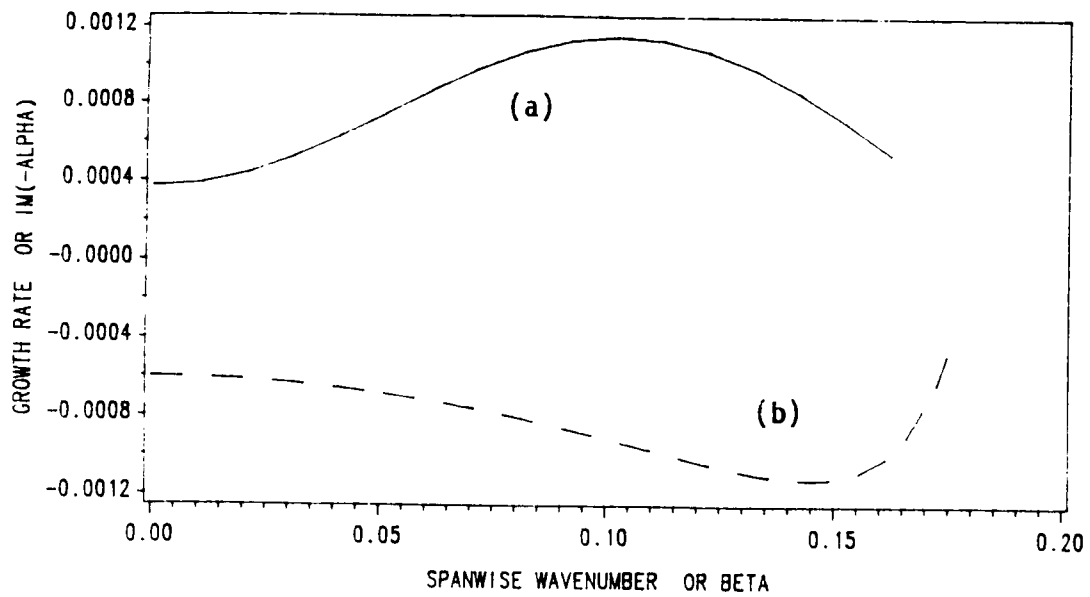
Figure 18. Variation of the growth rate of the free wave with spanwise wavenumber for $M_{\ni}$ = 4.5 and F = 60×10^{-3}: (a) first-mode wave at R = 1150, (b) second-mode wave at R = 1950.
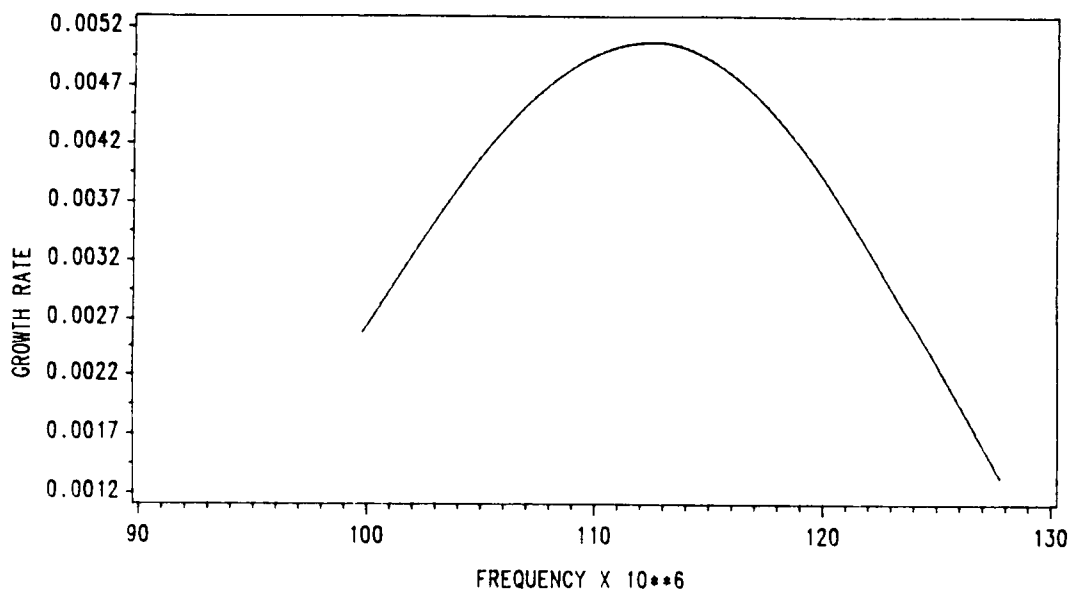
Figure 19. Variation of the secondary growth rate with frequency for B = 0.199, M_{∞} = 4.5, and R = 1950; the primary wave is a first-mode wave having an $a^{=}$ = $0.01/\sqrt{2}$.
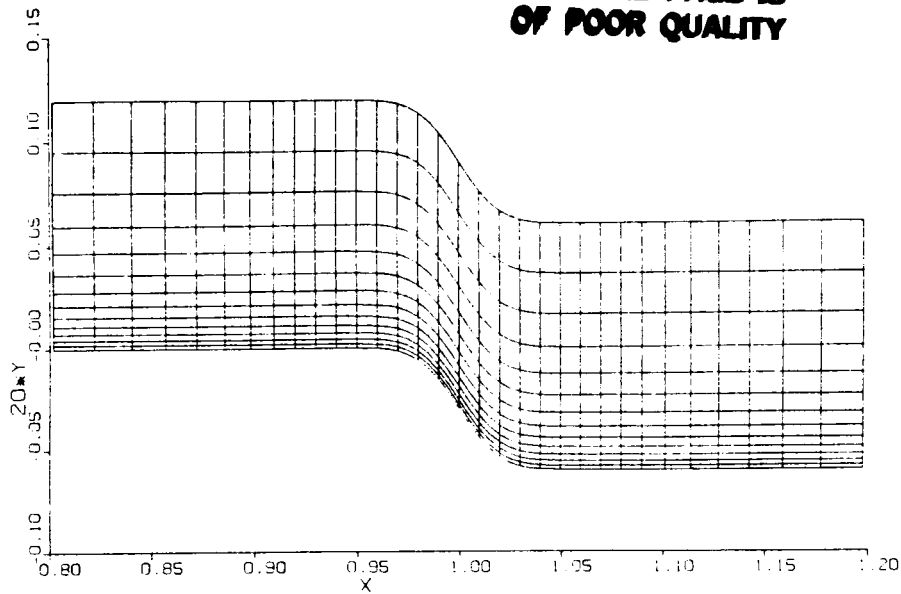
Figure 20.   A typical computational grid for a backward-facing step.
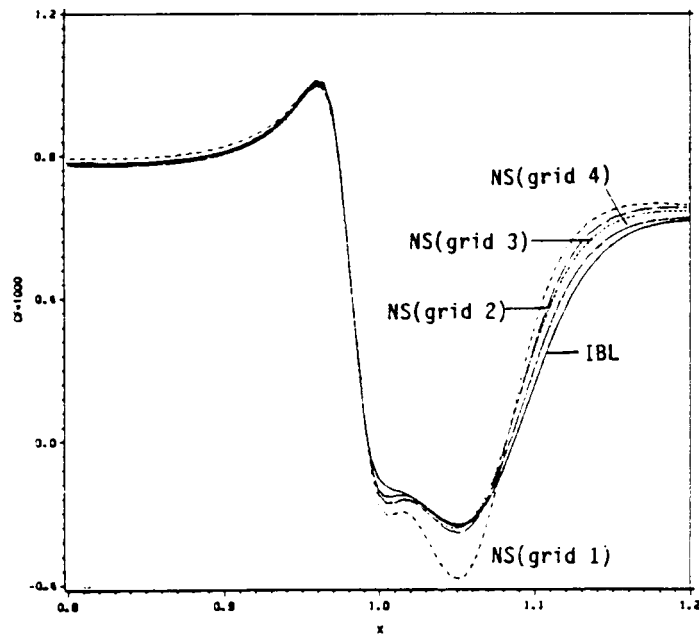
Figure 21.   The friction-coefficient distribution calculated over a backward-facing step whose height is -0.003 and center is at Re = 10^3 for an M_{∞} = 0.5.

Figure 22. Pressure-coefficient distribution calculated over a backward-facing step whose height is -0.003 and center is at Re = 10^5 for an M_∞ = 0.5: —— IBL, --- Navier-Stokes solver (grid 4).
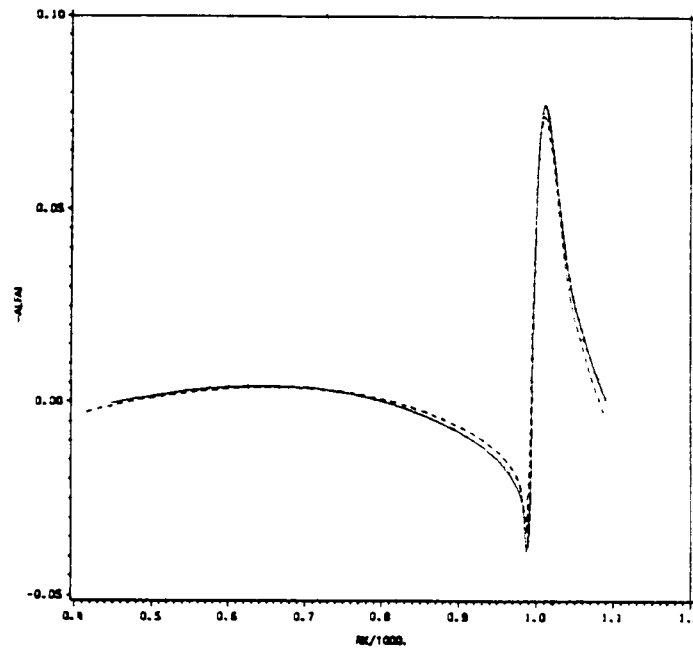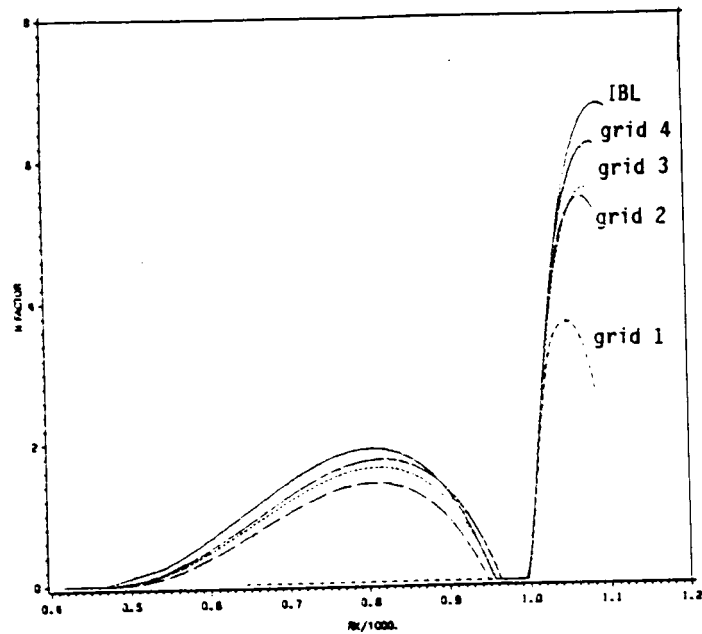

Figure 23. Spatial growth rates of 2D waves having the frequnecy 80×10^{-6} propagating over a backward-facing step whose height is -0.003 and center is at Re = 10^6 for an M_∞ = 0.5: —— IBL, --- Navier-Stokes solver (grid 4).

Figure 24. Amplification factor distribution over a backward-facing step whose height is -0.003 and center is at Re = 10^6 for an M_∞ = 0.5 and an F = 80×10^{-6}.
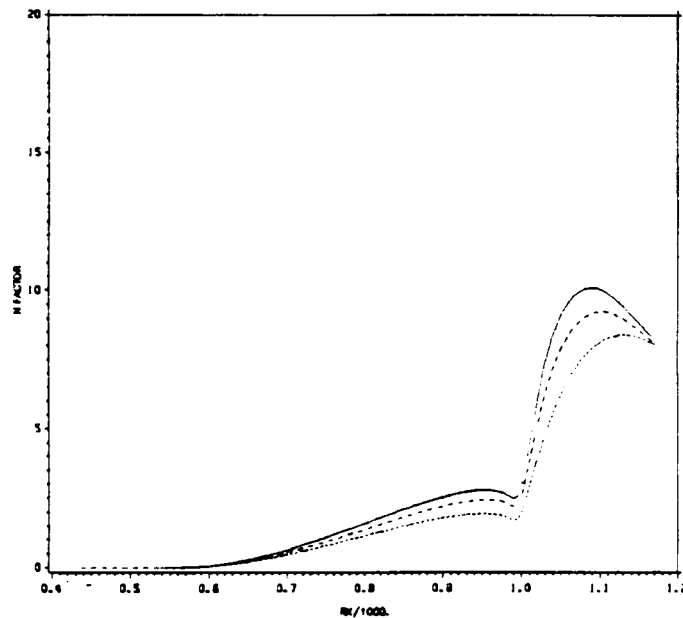

Figure 25. Influence of Mach number on the amplification factor of the most amplified 2D wave propagating over a backward-facing step whose height is -0.003, slope is -4.349°, and center is at Re = 10^5: —— M_∞ = 0.0, --- M_∞ = 0.5, ... M_∞ = 0.8.
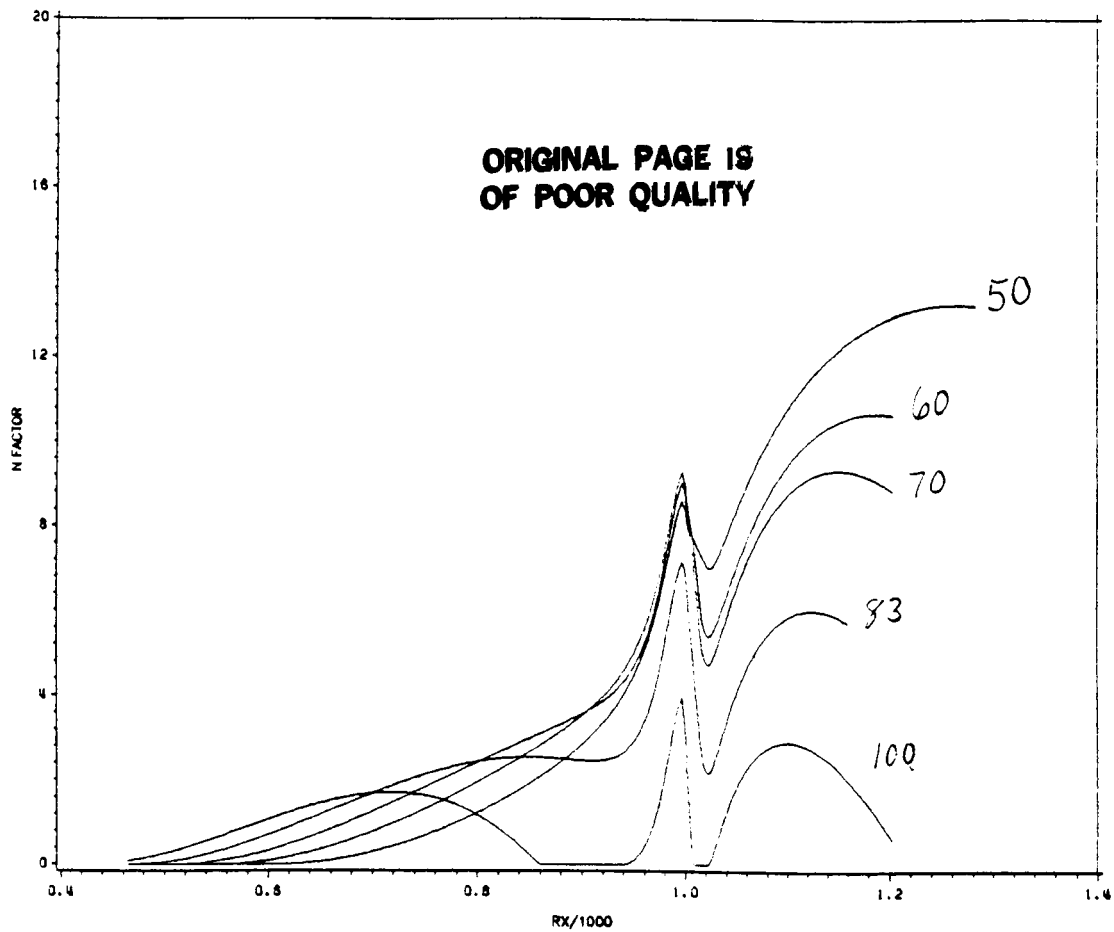
Figure 26. Variation of the N-factor distribution with frequency for waves propagating past a backward-facing step whose height is -0.003, slope is -4.349°, and center is at $Re = 10^6$; $M_\infty = 0.5$.